Naval Research Laboratory

Washington, DC 20375-5320

NRL/FR/8140--96-9813

Parametric Error Analysis of Tropospheric Propagation Effects

JUNHO CHOI

Command Control Communication Computer and Intelligence Branch
Space Systems Development Department

June 13, 1996

REPORT DOCUMENTATION PAGE

Form Approved
OMB No. 0704-0188

1. AGENCY USE ONLY (*Leave Blank*)	2. REPORT DATE	3. REPORT TYPE AND DATES COVERED
	June 13, 1996	

4. TITLE AND SUBTITLE

Parametric Error Analysis of Tropospheric Propagation Effects

5. FUNDING NUMBERS

6. AUTHOR(S)

Junho Choi

7. PERFORMING ORGANIZATION NAME(S) AND ADDRESS(ES)

Naval Research Laboratory
Washington, DC 20375-5320

8. PERFORMING ORGANIZATION REPORT NUMBER

NRL/FR/8140--96-9813

9. SPONSORING/MONITORING AGENCY NAME(S) AND ADDRESS(ES)

Space and Naval Warfare Systems Command
2451 Crystal Drive
Arlington, VA 22245-5200

10. SPONSORING/MONITORING AGENCY REPORT NUMBER

11. SUPPLEMENTARY NOTES

12a. DISTRIBUTION/AVAILABILITY STATEMENT

Approved for public release; distribution unlimited.

12b. DISTRIBUTION CODE

13. ABSTRACT (*Maximum 200 words*)

The effects of tropospheric radiowave propagation have been studied based on parametric approach and ray-tracing graphs with empirical data supplied by the National Climatology Data Center in Asheville, North Carolina. Correlation among parameters such as temperature, pressure, relative humidity, refractivity and elevation angles has been extensively investigated for effects on range errors and elevation angle errors. Studies of lapse rate, refractive index and time delays are also included for the completeness of relational functions among parameters that directly affect both range and angle of arrival errors. Results indicate that range and angle errors vary quite dynamically by season and month, and in region. The errors in the low-elevation angles less that 10° are higher than expected, and those errors should not be neglected for higher accuracy requirements.

14. SUBJECT TERMS

Climatology, Time delays, Angle of arrival, Troposhere, Refractivity, Elevation angle error, Range error, Lapse rate, Correlation, Meteorology, Refractive index

15. NUMBER OF PAGES

52

16. PRICE CODE

17. SECURITY CLASSIFICATION OF REPORT	18. SECURITY CLASSIFICATION OF THIS PAGE	19. SECURITY CLASSIFICATION OF ABSTRACT	20. LIMITATION OF ABSTRACT
UNCLASSIFIED	UNCLASSIFIED	UNCLASSIFIED	UL

NSN 7540-01-280-5500

Standard Form 298 (Rev. 2-89)
Prescribed by ANSI Std 239-18
298-102

CONTENTS

PARAMETRIC ERROR ANALYSIS OF TROPOSPHERIC PROPAGATION EFFECTS

INTRODUCTION

Background

The atmosphere extends from the surface of the Earth to several Earth radii where it merges with the interplanetary medium. Most of the atmosphere's mass is below a height of 12 km, which is within the tropospheric region. Compared with the mean radius of the Earth (6371 km), the bulk of the atmosphere is contained in a relatively thin layer. However, when this collection of viscous gases, water vapor, and floating particulate matter is acted upon by an equator-to-pole air temperature gradient, evaporation, condensation of water, the rotation of the Earth, and surface friction, it becomes a very complex physical system. In the mid-latitudes, our main appreciation of this physical system manifests itself in the passage of weather systems. While weather systems are relatively short term, rarely lasting more than seven days in any given location, they have a very large impact upon our way of life. The longer term effects of the atmospheric system are manifest in what we experience as climate. One of the continuing goals of atmospheric research is to be able to predict the motions of the atmospheric fluid over a wide range of scales. These scales include: small scale turbulence (1 cm to 1.0 km), the mesoscale system such as thunderstorms, tornadoes, and squall lines (1.0 km to 100 km), the synoptic scale characteristics such as weather systems (100 km to several thousand kilometers); as well as, climatic trends that occur over periods of hundreds of years and have a scale of tens of thousands kilometers [1].

The fundamental problems of atmospheric science become quite obvious. Primarily, the atmosphere is a continuum in time and space that contains motion systems, or eddies, in the frequency and wave number spaces. A representation of atmospheric motions in frequency space is provided, for instance, by spectrum analysis of wind speeds at jet-stream level over a single station, which reveal a spectrum of kinetic energy that shows several prominent wave bands and considerable variability with time and location of measurement, nevertheless it is uninterrupted and continuous throughout the frequency range accessible to detailed measurements. Yet, we are forced to apply simplified mathematical models that we call "theory" to relatively narrowbands within the spectrum of atmospheric motions.

A variety of explanations of tropospheric propagational problems have been presented based upon model-based or empirical measurements in terms of frequencies and climatic regions over the years [2-9]. However, important details relating to the properties of the received signal are generally less certain; such details might be signal amplitude, delay times between different paths, and individual angles of arrival under multipath conditions. Meteorological uncertainties severely limit the usefulness of models of existing microwave propagation; specifically in the presence of

Manuscript approved February 15, 1996.

precipitation. Many of the propagational problems on the line-of-sight links arise from the occurrence of anomalous departures in the vertical gradient and in the refractive index from the normal, almost steady value. This value will vary slowly with the season, time of day, location, and the standard gradient in refractivity often being quoted as –40 N-unit/km corresponding to a 4/3 Earth [10].

Even though there is evidence of tropospheric-stratospheric coupling and some evidence of extra-terrestrial influences upon tropospheric motions, generally in the form of slight variations of incoming solar radiation and tides in the atmosphere, the troposphere is almost a closed atmospheric system [1]. Thus, characteristics of this layer can be quantitatively deduced from measurements of variables within the layer itself. This quantitative deduction is made possible by simulating the general circulation of the atmosphere using basic or primitive equations that we define as:

a. mean atmospheric motions,
b. thermodynamic properties including phase change of water, and
c. conservation of mass, with the restriction upon the equations that the total system conserve energy.

However, the use of these primitive equations is severely hampered by inadequate knowledge of;

a. the initial conditions defining the atmospheric system, and
b. the boundary conditions acting upon the system.

The use of the primitive equations is also simplified by calculating solutions to the equations at specified grid points that are distributed vertically and horizontally over the globe. It is obvious that in such a scheme the number of points is important. Further, the spacing between the grid points determines the number of points used in the calculation of the various horizontal fields of motion, or in terms of pressure, temperature, and moisture at different vertical levels of the atmosphere. At present, both the observational system, which provides the initial conditions, and the numerical calculation system, which provides the forecast, are based upon grid points whose distance interval is much larger than the interval of motions present in the planetary boundary layer. Because of this spacing, the effects of these motions are lost to the calculation even though they are physically very important. Thus one of the principal tasks faced in atmospheric research is the parameterization of subgrid scale phenomena in terms of grid scale variables.

Major emphasis here is concentrated on the physical phenomena in the atmosphere using empirical data rather than on building models or analysis based on models developed. Most of the results presented in this report are directed to quantifying parameterization schemes, and to investigate relational phenomena between parameters such as: refractivity, angle error, range error, pressure, temperature, and relative humidity for larger areas than the subgrid levels which were presented in the previous report [11].

Purpose and Scope

The main objectives of this report are to present analytical results based on parameter correlations among pressure, temperature, relative humidity, refractivity, and gradient, as well as, to quantify classifications of ray-tracing patterns among parameter variations for wider regional climatological profiles. The result of this analysis may contribute to a better understanding of the principal atmospheric effects, which are refraction, absorption, and thermal noise generation with scintillation effects resulting from refractive-index irregularities and Faraday rotation of the plane of

polarization by the ionosphere. These factors mainly produce the range and elevation angle errors for radiowave propagation in the low atmosphere below 12 km. These range and elevation angle errors should be considered as known bias errors, since their magnitudes are calculable. The uncertainty of their exact magnitudes from simplifying assumptions concerning the state of the atmosphere is partly caused by unknown bias errors and partly by precision errors. These errors can be reduced if the pertinent atmospheric parameters are known in real-time or can be approximated for the propagation path with seasonal, monthly, diurnal, or annual statistical atmospheric data such as temperature, atmospheric pressure, and partial water vapor pressure.

The range and elevation angle errors with lapse rate phenomena are thoroughly investigated in both theoretical and empirical aspects of the tropospheric propagation correction, based on meteorological observed data for ten years on a monthly average. Later on in the report, "Temperature Lapse Rate," the temperature profiles are examined with empirical ray-tracing results. Refractive index structure is reviewed in section "Refractive Index Structure" to enhance understanding of the tropospheric propagation characteristics. In section "Range Errors," range errors are studied in both analytical and experimental aspects with comparison of several alternatives to correct inherent range errors. In section "Evaluation Angle Errors," angle errors are derived and tested with empirical data for angle error correction in a real system. In section "Correlation Analysis of Meteorological Parametric Variables," relational study among those parameters such as errors, refractivity, elevation angles, and atmospheric parameters is presented based upon ray-tracing graphs for several regional attributes. Finally, the conclusion and recommendations are presented in section "Conclusions" with references in section "References." No attempt has been made to provide a complete list of all important papers or text books on the subject, since they are far too numerous to include in the single section of references of a short report like this one.

TEMPERATURE LAPSE RATE

The background temperature of the real atmosphere is not a constant, but rather varies substantially on a scale of a few kilometers in the vertical structure of the troposphere. One can infer the quality of the consequences of this by considering an elementary case in which one isothermal half-space is superimposed to another of different temperature, there will be a wave incident upon the interface from below. The actual temperature profiles, smoothly varying, give rise to continuous processes of refraction and internal reflection, with the result of interference effects that can be complex but must be adequately treated in some detail if at all adequately. Temperature decreases with the increasing altitude in the troposphere, on the average, but temperature inversion layers provide exceptions to this general characteristic. The lapse rate of temperature that occurs in homogenous air is called the adiabatic lapse rate, because it represents the decrease of temperature of an air parcel which rises and cools adiabatically. If the air is unsaturated, the temperature decreases with height and is properly called the dry adiabatic lapse rate. In practice, however, it is often referred to simply as adiabatic lapse rate. If condensation or evaporation processes occur, latent heat is a factor; the lapse rate under this condition is called the moist-adiabatic lapse rate or saturation-adiabatic lapse rate.

The rate of change of temperature with altitude is analyzed below using the first law of thermodynamics which is functionally described by

$$dQ = c_p dT - \alpha dp \tag{1}$$

where c_p is the specific heat of dry air at constant pressure, α the specific volume of the gas (the inverse of the air density (ρ)), p the atmospheric pressure, T the absolute temperature in Kelvin and

dQ an increment of sensible heat [Grossman, Chapter 1 in [1]]. One can derive another important atmospheric variable called the potential temperature by assuming that Eq. (1) describes an adiabatic process. An adiabatic process is one in which no sensible heat is exchanged into or out of the thermodynamic system under consideration. In this case the thermodynamic system is an atmospheric parcel. With this assumption Eq. (1) can be rewritten as

$$c_p dT - \alpha dp = 0. \tag{2}$$

From the law of ideal gas the atmospheric pressure becomes

$$p = \rho RT \tag{3}$$

where R is the specific gas constant for dry air equal to 0.28704 J g^{-1} K^{-1}.

Combining Eqs. (2) and (3),

$$dT/T - (R/c_p)\, dp/p = 0. \tag{4}$$

If we integrate both sides and p_o is taken to be 1000 mbar while the notation for T_o at that pressure is replaced to Q, we then have

$$\Theta = T(p/1000)^{R/c_p} \tag{5}$$

which is the equation for the potential temperature [12]. The potential temperature is a conservative quantity (i.e., does not change with either time or displacement) for adiabatic processes in the atmosphere and for this reason is often used in tracing atmospheric motions.

If we assume that

a. there is no vertical acceleration of the air,
b. with the air parcel in motion, frictional or stress forces are small, and
c. forces due to the rotation rate of the Earth are negligible (i.e., assuming no vertical acceleration of the air and the effect of gravity on a unit volume of air is balanced by the difference in pressure above and below the unit volume), the hydrostatic equation can be written as

$$dp/dz = -\rho g \quad \text{or} \quad \alpha dp = -g dz \tag{6}$$

where z is the zenith height, g the gravity acceleration, and ρ the density of gas. If we combine and rearrange Eqs. (3), (4), and (6) with the assumption of no water vapor,

$$dT/T + (R/c_p)(g/RT)dz = 0. \tag{7}$$

By rewriting this equation we obtain.

$$\Gamma = -dT/dz = g/c_p = 9.76^{\circ}\ \text{K/km} \tag{8}$$

where Γ is known as the dry adiabatic temperature lapse rate. Since, in general, temperature in the troposphere or the lower atmosphere decreases with increasing altitude, the following convention is used

$$\gamma \equiv - dT/dZ \tag{9}$$

where γ is defined as the lapse rate of temperature. Therefore negative γ indicates increasing temperature with increasing altitude. Two important points should be made with reference to Eq. (8). The first is that due to the adiabatic assumption, an atmospheric layer with $\gamma = \Gamma$ has no sensible heat flux into or out of the layer. The second point is that since the potential temperature Θ must be constant in an adiabatic process, layers which have $\gamma = \Gamma$ also have $d\Theta/dz = 0$. It is often stated that layers with the above properties are well mixed layers.

Equations (8) and (9) can provide the atmospheric stability depending upon the following criteria:

If $\gamma > \Gamma$, the atmosphere is unstable, since vertical acceleration of the air parcel in the direction of displacement from z_o will result. If $\gamma < \Gamma$, the atmosphere is stable while $\gamma = \Gamma$ indicates the neutral state.

Hopfield in [2] used the temperature lapse rate when she introduced the two-quartic tropospheric correction model for both dry and wet refractivity in terms of the height (or altitude) by introducing a new exponent parameter as,

$$\mu = [g/(R\gamma)] - 1. \tag{10}$$

By plotting the relation between μ and γ of Eq. (10) [8] it is clear why Hopfield chose $\mu = 4$; $\gamma = 6.71$, which is optimum in the sense of lower elevation angle ($> 10^{\circ}$) and in the state of the stable atmospheric condition.

Above the surface layer, the gradient of potential temperature vanishes. Thus, the bulk of the boundary layer (100 to 1000 m) has an almost uniform potential temperature, Eq. (5). The top of the boundary layer is usually marked by a temperature inversion. This temperature inversion is caused by the turbulent mixing of the air from below with the warmer air above. This results in a downward heat flux in the upper part of the boundary layer. The height of the inversion layer depends on several factors such as the total amount of heat that entered the atmosphere at the Earth's surface during the day, the lapse rate of the undisturbed air above the temperature inversion, large scale convergence or divergence, etc. Temperature fluctuations have a characteristic structure. It is clear that with increasing height the quiescent periods become longer and the total variance decreases. The vertical velocity structure is quite different. The fluctuations appear to be much closer to a normal distribution and the variance increases with height in the surface layer and reaches a maximum at about 200 to 300 m [J.A. Businger, Chapter 6 in [1]]. Temperature inversions have a twofold importance,

a. they can be widespread in area and persist over a relatively long period of time, and
b. they exercise a stabilizing influence on air motion so that turbulence is suppressed and strong humidity gradients may develop.

Layers where there is intense superrefraction to the point of duct formation may be formed as a result of these gradients, and trapping of radio waves may follow. The temperature inversions may start at the ground level or at some greater height. The thickness of the layer can show great variability.

Several different temperature profiles in the atmosphere are presented with different sizes of coverage and geographical locations. Figure 1 shows the ray tracing graphs for

a. the size of 2.5° × 2.5° grid,
b. 7.5° × 7.5° grid,
c. Eastern U.S. region
d. global, and
e. ocean areas of the East Coast of U.S. for the comparison of local temperature changes with regional and global variations.

As can be seen from Fig. 1, super adiabatic layer (from the surface to approximately 12 km in the atmosphere) variation is very similar in each graph, while temperature convection layer (from 12 km to 21 km) varies with sharp increases or gradual increases and even flat like in ocean or East U.S. regions. Similarly, the temperature inversion layer (from zero variation to positively upward) and stable region (where the lapse rate increases positively) varies depending upon the small areas as in Fig. 1(a) and 1(b) or large areas like Fig. 1(c) and 1(e). It is noticed that the global lapse rates are very close to each other for four seasons while ocean and Eastern U.S. areas are clearly different from season to season. When these kinds of data are applied to RF propagation areas, it is natural to ask whether it is appropriate for the adoption of the global data or if data should be applied locally and seasonally or possibly diurnally rather than based on annual climatological data.

Figure 2 shows a variety of regional profiles from the Florida peninsula to the Great Lakes, mountains, and plains. Figures 2(a) (marsden square 2, latitude 32.5° to 42.4° N and longitude 70.0° to 80.0° W), 2(d) (marsden square 7, latitude 37.5° to 47.5° N and longitude 95.0° to 105.0° W), and 2(e) (marsden square 3, latitude 32.5° to 42.5° N and longitude 75.0° to 85.0° W) show some variations by season while Figs. 2(b) (Southeast U.S. region 1, latitude 22.5° to 32.5° N and longitude 95.0° to 105.0° W), 2(c) (Southeast U.S. region 2, latitude 22.5° to 42.5° N and 85.0° to 95.0° W) and 2(f) (Southeast U.S. region 3, latitude 22.5° to 32.5° N and longitude 75.0° to 85.0° W) are close to each other throughout the year. This may be construed that temperature variations in the southern latitude are smaller than those of the northern latitude, inlands and mountain areas.

Figure 3 shows the vertical temperature profiles vs the pressure level for different parts of the Earth from the tropical region to the North American continent and Asian continent. It is noticed that the lapse rates vary dynamically depending on regions and seasons. It is also clear that the inversion processes or layers are sharply different from regional and seasonal basis. For example, Fig. 3(b) (Europe, latitude 35.0° to 60.0° N and longitude 15.0° to 30.0° E) reveals longer convection layer processes than inversion processes while Figs. 3(f) (Northwest Pacific, latitude 5.0° to 22.5° N and longitude 135.0° to 155.0° E), and 3(c) (Persian Gulf, latitude 10.0° to 45.0° N and longitude 30.0° to 70.0° E) present shorter convection layer and longer inversion layer processes with similar behavior for four seasons. It is interesting to notice that Figs. 3(d) (East U.S., latitude 32.5° to 47.5° N and longitude 65.0° to 90.0° W) and 3(e) (West U.S., latitude 30.0° to 52.5° N and longitude 100.0° to 130.0° W) show the middle ground among the previous extreme for the aspects of convection layer and the inversion layer.

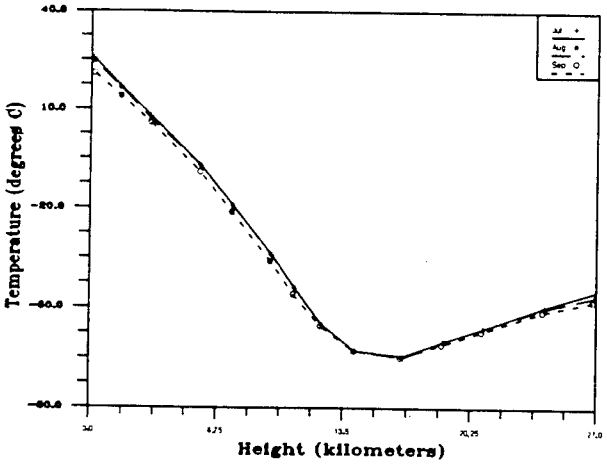

(a) — Height vs temperature, DC July, August, September, ECM database, 10 year average

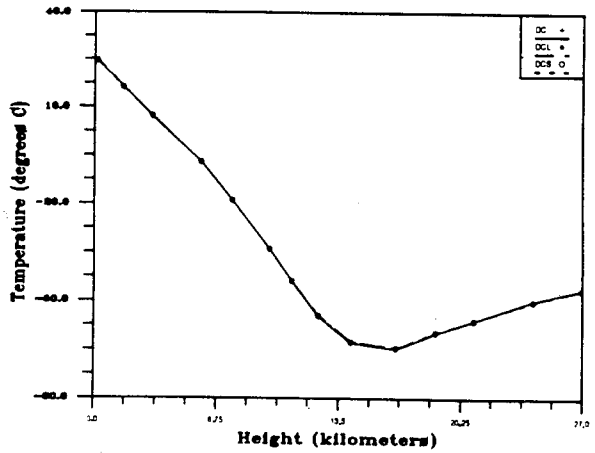

(b) — Height vs temperature, DC, DC Land, DC Sea, August ECM database, 10 year average

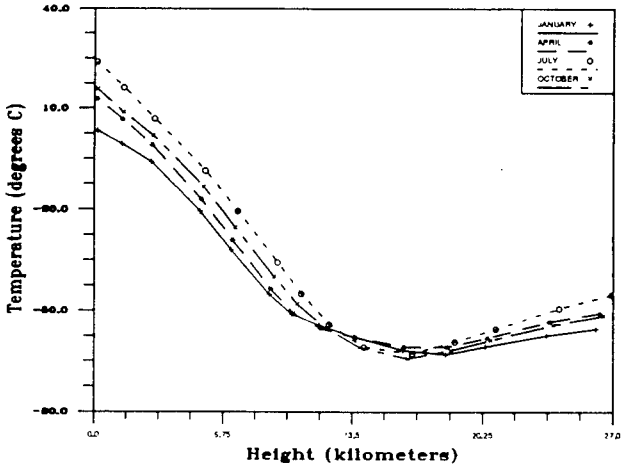

(c) — Height vs temperature, Eastern U.S., ECM database, 10 year average

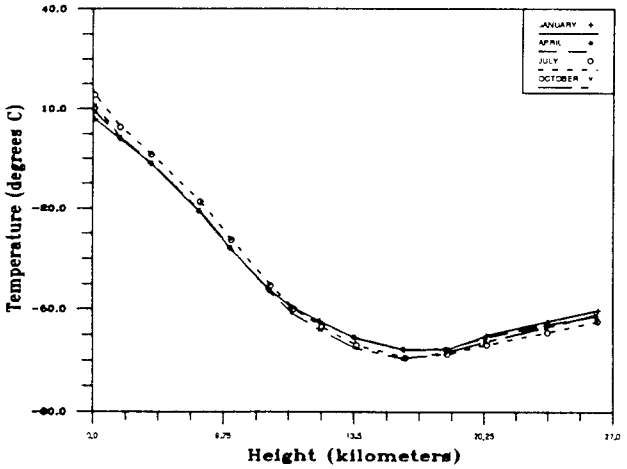

(d) — Height vs temperature, global, ECM database, 10 year average

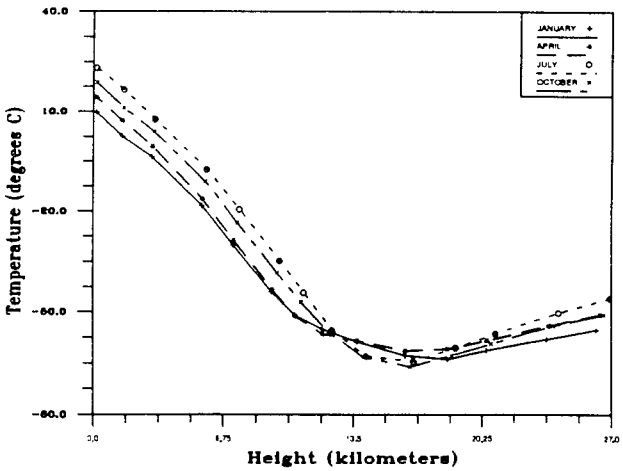

(e) — Height vs temperature, ocean, ECM database, 10 year average

Fig. 1 — Mean monthly temperature profiles over 10 year, between 1980-1991: (a) Washington, DC area, (b) nine grids areas surrounding Washington, DC, (c) global profiles, (d) 15 grids covered over Eastern U.S. coastal areas, and (e) 60 grids covered over Eastern U.S.

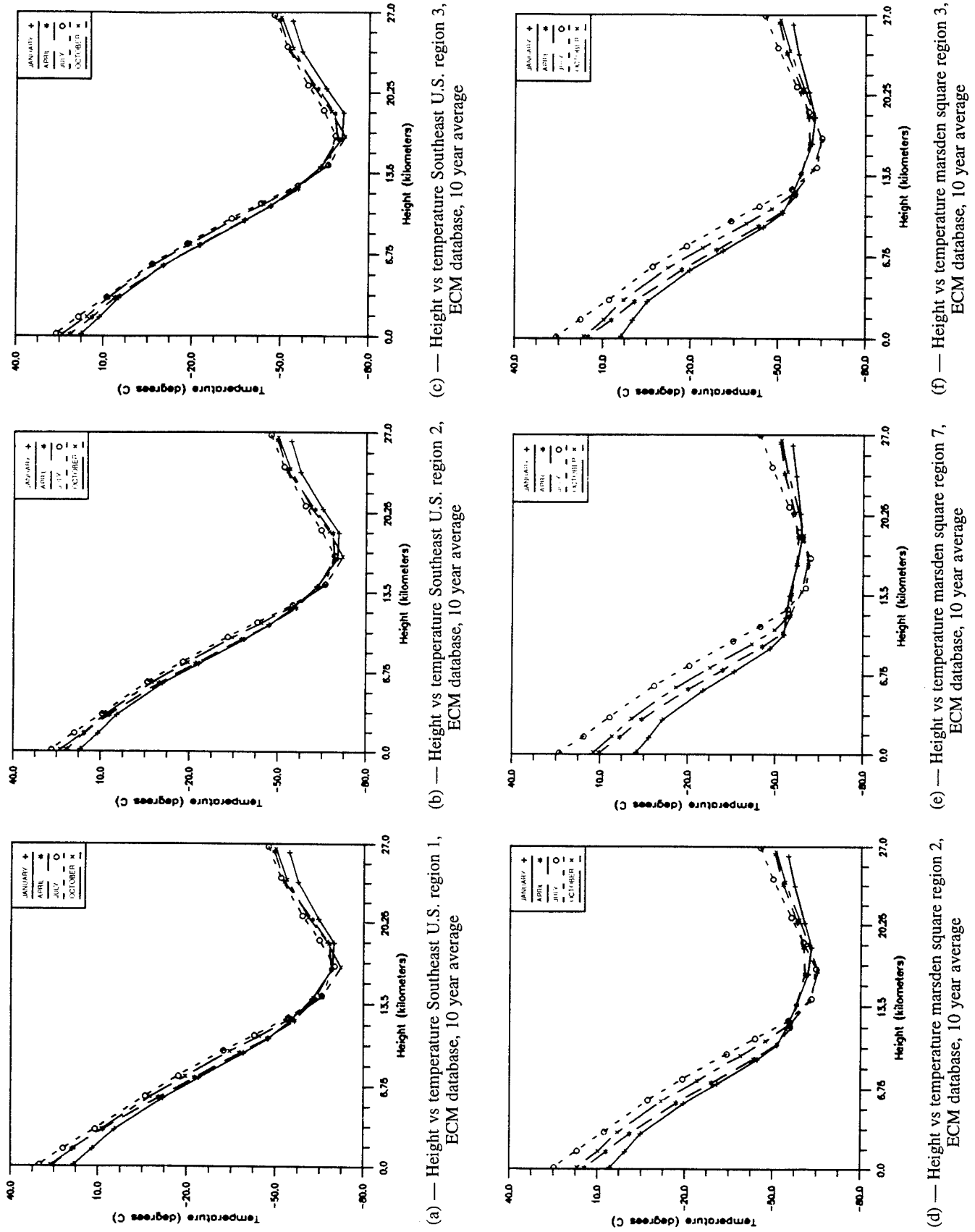

(a) — Height vs temperature Southeast U.S. region 1, ECM database, 10 year average

(b) — Height vs temperature Southeast U.S. region 2, ECM database, 10 year average

(c) — Height vs temperature Southeast U.S. region 3, ECM database, 10 year average

(d) — Height vs temperature marsden square region 2, ECM database, 10 year average

(e) — Height vs temperature marsden square region 7, ECM database, 10 year average

(f) — Height vs temperature marsden square region 3, ECM database, 10 year average

Fig. 2 — Mean monthly temperature profiles for marsden squares over different regions: (a) Atlantic coast, (b) Southeast-Texas neighborhood, (c) Gulf coast, (d) Great Lakes areas, (e) Appalachian mountain, and (f) Florida peninsula and surrounding coastal region.

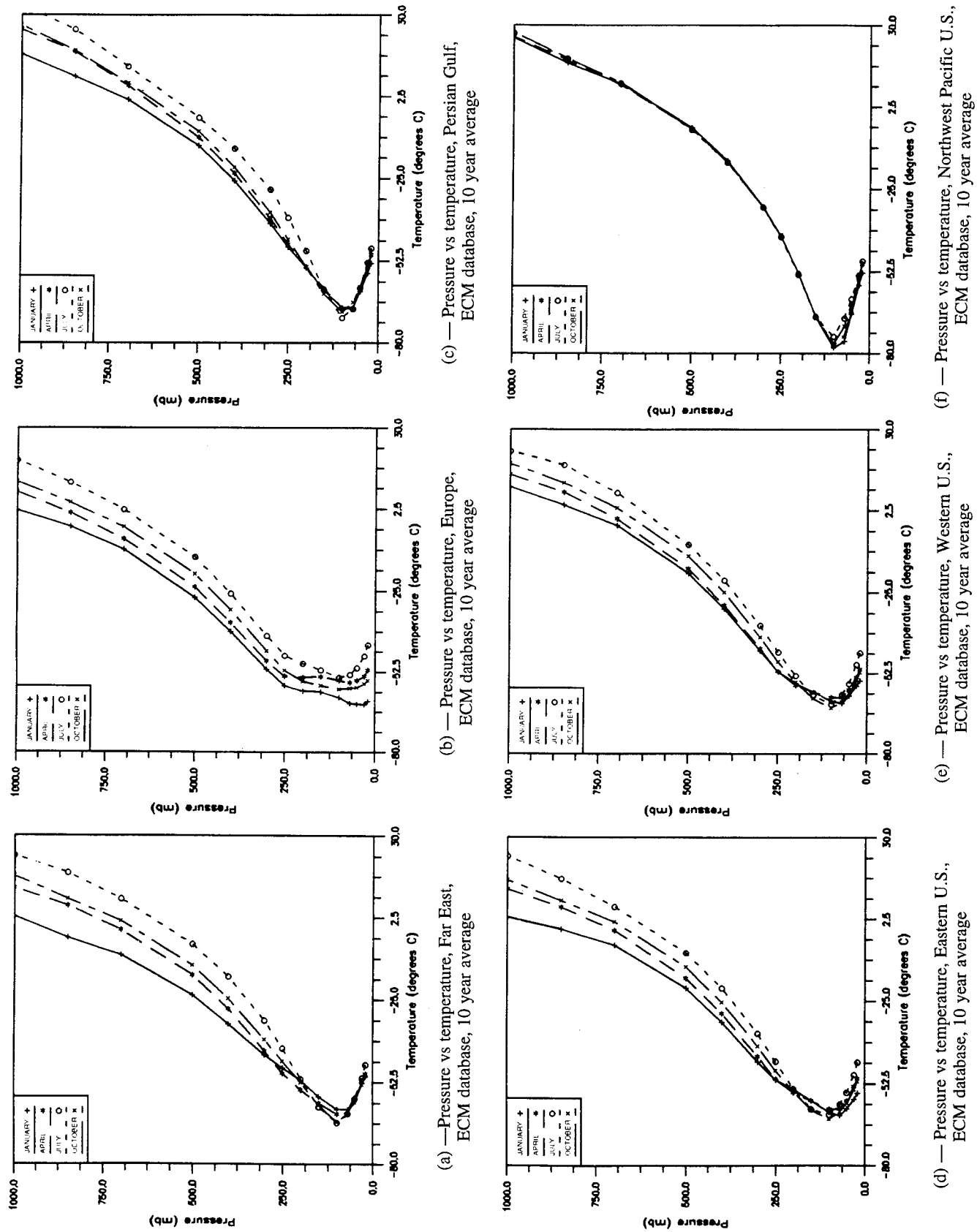

(a) —Pressure vs temperature, Far East, ECM database, 10 year average

(b) — Pressure vs temperature, Europe, ECM database, 10 year average

(c) — Pressure vs temperature, Persian Gulf, ECM database, 10 year average

(d) — Pressure vs temperature, Eastern U.S., ECM database, 10 year average

(e) — Pressure vs temperature, Western U.S., ECM database, 10 year average

(f) — Pressure vs temperature, Northwest Pacific U.S., ECM database, 10 year average

Fig. 3 — Mean monthly temperature profiles over atmospheric pressure variations: (a) Eastern U.S., (b) Western U.S., (c) Northwest Pacific areas, (d) Far East Asia, (e) Western Europe, and (f) Persian Gulf.

REFRACTIVE INDEX STRUCTURE

The radio refractive index is defined as the ratio of the speed of propagation of radio energy in a vacuum to the speed in a specified medium. The change in velocity of a radiowave has a direct effect on the measurement of distances using propagation time; whereas, the deviation of the vertical angle is proportional to the rate of change of velocity with altitude [5]. These errors can be reduced if pertinent atmospheric parameters, such as temperature, atmospheric pressure, and water-vapor pressure, are known, or measured directly by radiosonde, or can be approximated by the mathematical model for the propagation path. Spatial variations in these parameters with increasing heights cause refraction and lead to substantial refraction of RF waves in the lower atmosphere. The lateral extent of the effect of this refraction is determined by the homogeneity of the surrounding atmosphere. Thus, propagation modeling must account for vertical and horizontal structures of the atmosphere.

The path followed by a radio ray in the atmosphere is dependent upon the gradient of the refractive index along that path. Of the vertical and horizontal gradient components that compose the path gradient, the horizontal gradient is most often negligibly small for a certain degree of elevation angle. Thus, the atmosphere has been considered horizontally homogeneous and only the vertical gradient of the refractive index has been used. This assumption has been examined in this report (for low elevation angles below 5°) for validation in real world applications. The problem of determining the vertical and horizontal distribution of the refractive index of the troposphere for RF waves has engaged the attention of radio meteorologists [13]. Such information of refractive index distribution is vital to procedures and techniques for forecasting the radio refractive index profiles. The surface value and the gradient of the refractive index are important factors in the prediction of monthly median values of field strength over communication links using frequencies from 30 MHz to 50 GHz.

All time delay measurements are subject to the same primary sources of error, which are: uncertainty in the length of the long baseline required, incomplete knowledge of the refractive index along the path, and timing errors in the detection system. It should be emphasized that the group velocity is measured, and not the desired phase velocity. Therefore, another small correction (the order of 1 part in 10^5) is required to relate the speed of the light c that is perhaps the most important of all the physical constants. Aside from its many uses as the propagation velocity of electromagnetic waves, it plays a fundamental role in several branches of physics. The magnitude of this correction is obtained from the relation

$$v_g = d\omega/dk, \tag{11}$$

where v_g is the group velocity, w the angular frequency ($2\pi f$), and the wave number $k = 2\pi/\lambda$, λ being the wavelength. For electromagnetic waves,

$$\omega = k\, v_p \tag{12}$$

and

$$v_p = c/n \tag{13}$$

where

- v_p is the phase velocity, and
- n is the refractive index of the medium.

Note that the refractive index n is a phase refractive index linked to the phase velocity of the waves. It is also noticed that the refractive index is a function of the distance or range from the center of the spherical symmetry with the assumption of a permeability 1. Strictly speaking, the true refractivity n should be corrected by a modified version of $n(r)$ with some multiplicative factor such as r/r_o with r_o being the Earth radius. The phase velocity therefore can be greater than the velocity of light c when the refractive index is smaller than unity and is a minimum at the level of maximum ionization density in the ionosphere region. If the appropriate substitutions are made, the group velocity can be expressed by, [14]

$$v_g = v_p\,[1 + (\lambda/n)(dn/d\lambda)]. \tag{14}$$

If $dn/d\lambda = 0$, then $v_g = v_p$. The correction term is significant at optical wavelengths, but it is usually negligible for radio and microwave frequencies. The propagation velocity of electromagnetic waves refers, here, to the phase velocity that describes the RF propagation through the atmosphere of the Earth.

The atmosphere is the gaseous envelope of the Earth. It extends from the surface to the tropopause region. The method for calculating the index of refraction from the composition and physical parameters of a gas is given by, [15]

$$n - 1 \propto \rho\,(A + B/T) \tag{15}$$

where

- n is the refractive index,
- ρ the density of gas, and
- T is the temperature.

The first term is from the induced polarization of the gas molecules in the external field, and the second term from the permanent dipole moment of the molecules. For a mixture of gases, the index of refraction obeys the additivity rule, that is , the total value of $n - 1$ is equal to the sum of the contributions of the individual gases weighted in proportion to their partial pressures. The parameter B equals to zero for all gases in air, except water vapor, which has a dipole moment. The parameter A depends on dry gases and water vapor.

Many scientists proposed different values of parameters A, B, and ρ [5, 15, 16]. Since Smith and Weintraub in [17, 18] formulated the refractive index (i.e. Eq. (16)) through various experiments, the refractive index expression in Eq. (16) is adopted by CCIR in [19] and is in widespread use by radio scientists throughout the world as

$$n - 1 = (77.6/T)\,[p + 4810*e/T]*10^{-6} \tag{16}$$

where

- T is the air temperature in Kelvin,
- p the atmospheric pressure in millibars, and
- e the partial pressure of water vapor in millibars.

The first term of Eq. (16) applies to both optical and radio frequencies and is called a dry refractivity, while the second term is the explicit water vapor relationship required only at radio

frequencies and is called a wet refractivity. The partial pressure of water vapor can be expressed in terms of relative humidity as follows, [20]

$$e = RH * 6.105 * \exp(x) \tag{16(a)}$$

where

$$x = 25.22 * (T - 273.2)/T - 5.32 * \log_e (T/273.2) \tag{16(b)}$$

- p = atmosphere's barometric pressure in millibars
- T = atmosphere's absolute temperature in Kelvin
- RH = atmosphere's relative humidity in percentage

The radio refractivity N that is generally used to describe the spatial and temporal variations of the refractive index n is defined for convenience as

$$N = (n - 1) * 10^6. \tag{17}$$

Combining Eqs. (16) and (17), the most common expression of refractivity can be derived as

$$N = (77.6/T) [p + 4810*e/T] \tag{18}$$

where the first term represents the dry refractivity and the second term is referred to the wet refractivity, since the water vapor pressure is more dominant over temperature and pressure. At very low temperatures, the wet refractivity component becomes very small even for saturated air, and so the N is almost independent of relative humidity. As the temperature rises, there is a slow decrease in the dry refractivity N_d, but a rapid increase in the saturated value of the wet refractivity N_w. At high temperatures, variation of N_w can become somewhat larger than that of N_d, and so N varies considerably with relative humidity. At high temperature and high relative humidity, N is very sensitive to small changes in temperature and relative humidity. Consequently, the variability of N in tropical areas is far greater than that in cold climates such as continental temperate or polar climates.

Hopfield in [2] proposed the refractivity profile expression for the dry refractivity N_d, and wet refractivity N_w in terms of height variations based on a lapse rate of 6.7°C/km. As pointed out in the previous section, this lapse rate varies depending on the time of the day, geographical location, and direction of the look angle. Both dry and wet refractivity profile derived by Hopfield are given as:

$$N_d = k_d (h_{od} - h)^4 \qquad \text{for } h \le h_{od} \tag{19}$$

$$N_w = k_w (h_{ow} - h)^4 \qquad \text{for } h \le h_{ow} \tag{20}$$

where k_d and k_w are determined for any specific time, from this height, and the locally observed surface conditions. The parameter h_{od} and h_{ow} represent the equivalent height above the geoid for the dry and wet component respectively. The total theoretical refractivity N profile is then the sum of the two components, and the complete expression becomes

$$N = \sum_{i=1,2} N_i$$

$$N_i = [N_{Ti}/(h_{oi} - h_T)^4] * (h_{oi} - h)^4 \qquad \text{for } h \le h_{oi} \qquad (21)$$

$$N_i = 0 \qquad \text{for } h > h_{oi}$$

where i = 1, 2 refers to the dry and wet components respectively. All heights are measured above the geoid. The subscript T refers to the tracking station.

In the past, other approaches for dry and wet refractivity calculations were proposed in addition to the Hopfield model in [4, 6, 8, 17]. Many other exponential models were directed to compute the refractivity with respect to the height above the reference or scale height, which is calculated by the refractivity reached to 1/e of the surface refractivity.

Figure 4 shows the plots of dry refractivity, wet refractivity and total refractivity, with height in the vicinity of Washington, DC area for the month of July 1994. In the figure NLAT implies the Northern latitude and ELON the East longitude. As can be seen in the Fig. 4, the dry refractivity behaves similarly for both small local area and larger local region while the wet refractivity behaves quite differently for each region and time of the day. Figure 4(a) shows the refractivity of dry, wet and total component for the morning in the west of the Washington, DC, while Fig. 4(b) represents those of the afternoon for the same area in July 1994. Figure 4(c) plots expanded areas of the west part of Washington, DC vicinity with nine grids. In the meantime, Figs. 4(d) and 4(e) show the dry- wet- and total-refractivity in the eastside of Washington, DC vicinity for the morning and afternoon respectively. Finally, Fig. 4(f) shows the graph of the dry- wet- and total-refractivity for the larger extent of the eastside of Washington, DC vicinity in the morning portion of July 1994. As noticed from these plots, the wet refractivity affects more than 30% of the dry refractivity below 3,000 ft above the ground surface. When it passes around 10,000 ft, the wet component occupies less than 10% of the dry refractivity.

Figure 5 shows the refractivity variations with height for the single marsden square by seasonal and different regions. Figure 5(a) covers the mid-Atlantic area with latitude 32.5° to 42.5° N and longitude 70° to 80° W for 50% of land and 50% of ocean area. Figure 5(b) covers the Eastern U.S. with latitude 32.5° to 47.5° N and longitude 65° to 90° W. Figure 5(c) covers most of the Florida peninsula with latitude 22.5° to 32.5° N and longitude 75° to 85° W. Figure 5(d) shows the ray-tracing plots of the empirical data for latitude 37.5° to 47.5° N and longitude 75° to 85° W which covers most areas of the Great Lakes. Figure 5(e) covers latitude 37.5° to 47.5° N and longitude 70° to 80° W for New England coastal areas. Figure 5(f) covers the mountain and coastal area of mid-latitude with latitude 32.5° to 42.5° N and longitude 75° to 85° W. It is noticed that refractivity of the lower latitude is higher than the refractivity at upper latitudes like New England and Great Lakes areas throughout the all year. Also, it is important to note that the refractivity below about 5.5 km in space varies by season while the refractivity above about 5.5 km in space does not change too much seasonally.

One of the most significant observations for the influence of the troposphere on radiowave propagation is the large-scale variation of refractive index with height, and the extent to which this changes with time. Variation of refractive index in the horizontal direction is almost negligible in comparison with the vertical variation. Such localized changes of refractive index with height cause ducting and reflection from elevated layers. The observed refractivity distribution is more nearly an

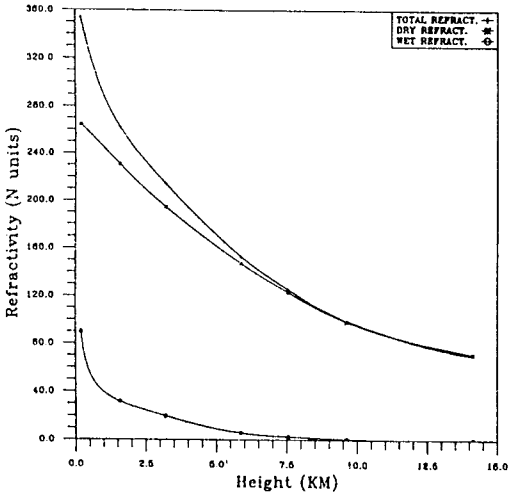

(a) — Refractivity N vs height, DC July AM average, FNMOC, SQR = 2273, NLAT = 37.5 -40, ELON = 280-282.5, 1994

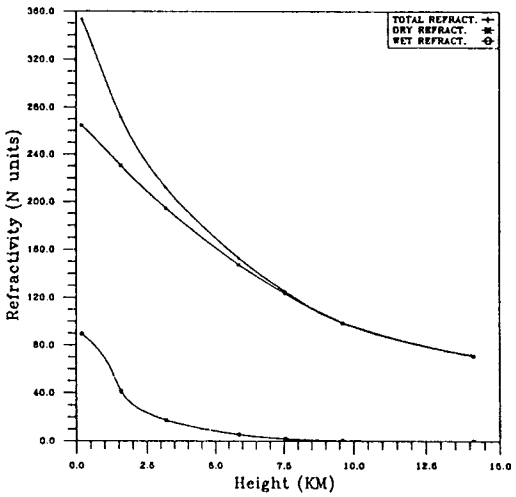

(b) — Refractivity N vs height, DC July PM average, FNMOC, SQR = 2273, NLAT = 37.5 -40, ELON = 280-282.5, 1994

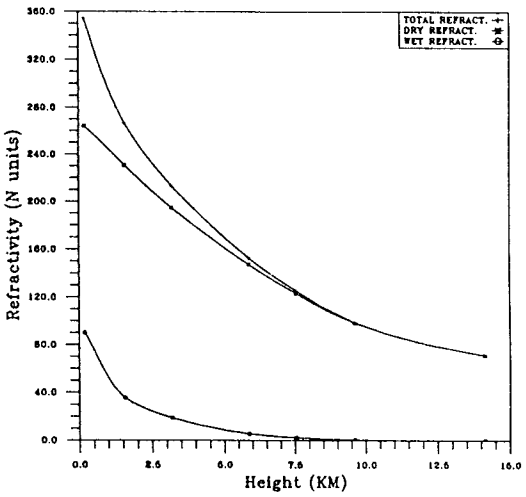

(c) — Refractivity N vs height, DC, land region, July AM average, FNMOC, NLAT = 35-42.5, ELON = 277.5-285, 1994

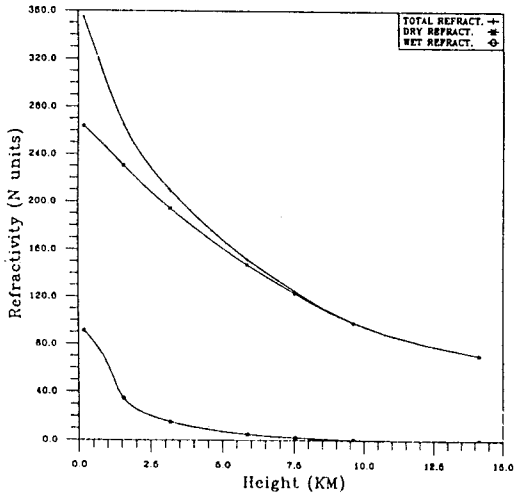

(d) — Refractivity N vs height, DC July AM average, FNMOC, SQR = 2274, NLAT = 37.5 -40, ELON = 282.5-285, 1994

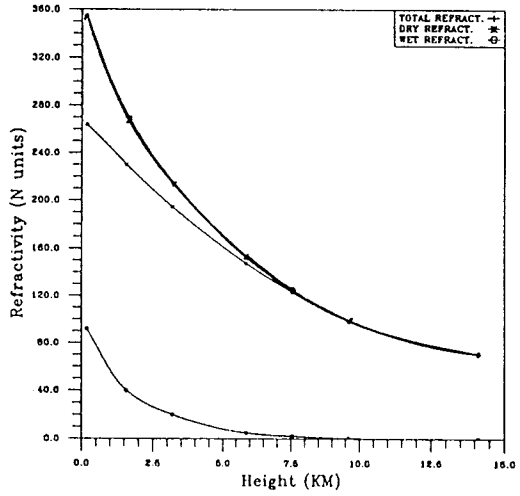

(e) — Refractivity N vs height, DC July PM average, FNMOC, SQR = 2274, NLAT = 37.5 -40, ELON = 282.5-285, 1994

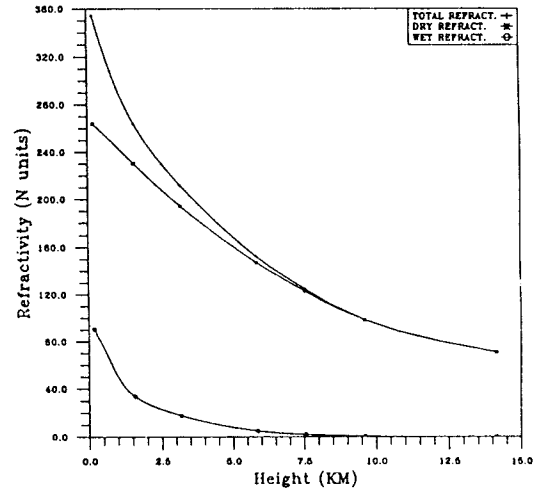

(f) — Refractivity N vs height, DC coastal land region July AM average, FNMOC, NLAT = 35 -42.5, ELON = 280-287.5, 1994

Fig. 4 — Refractivity in the vicinity of Washington, DC, July 1994: (a) the west part of DC, AM, (b) the west part of DC, PM, (c) 9-grids areas of the west part of DC, AM, (d) the east part of DC, AM, 3(e) the east part of DC, PM, and (f) 9-grids areas of the east part of DC AM.

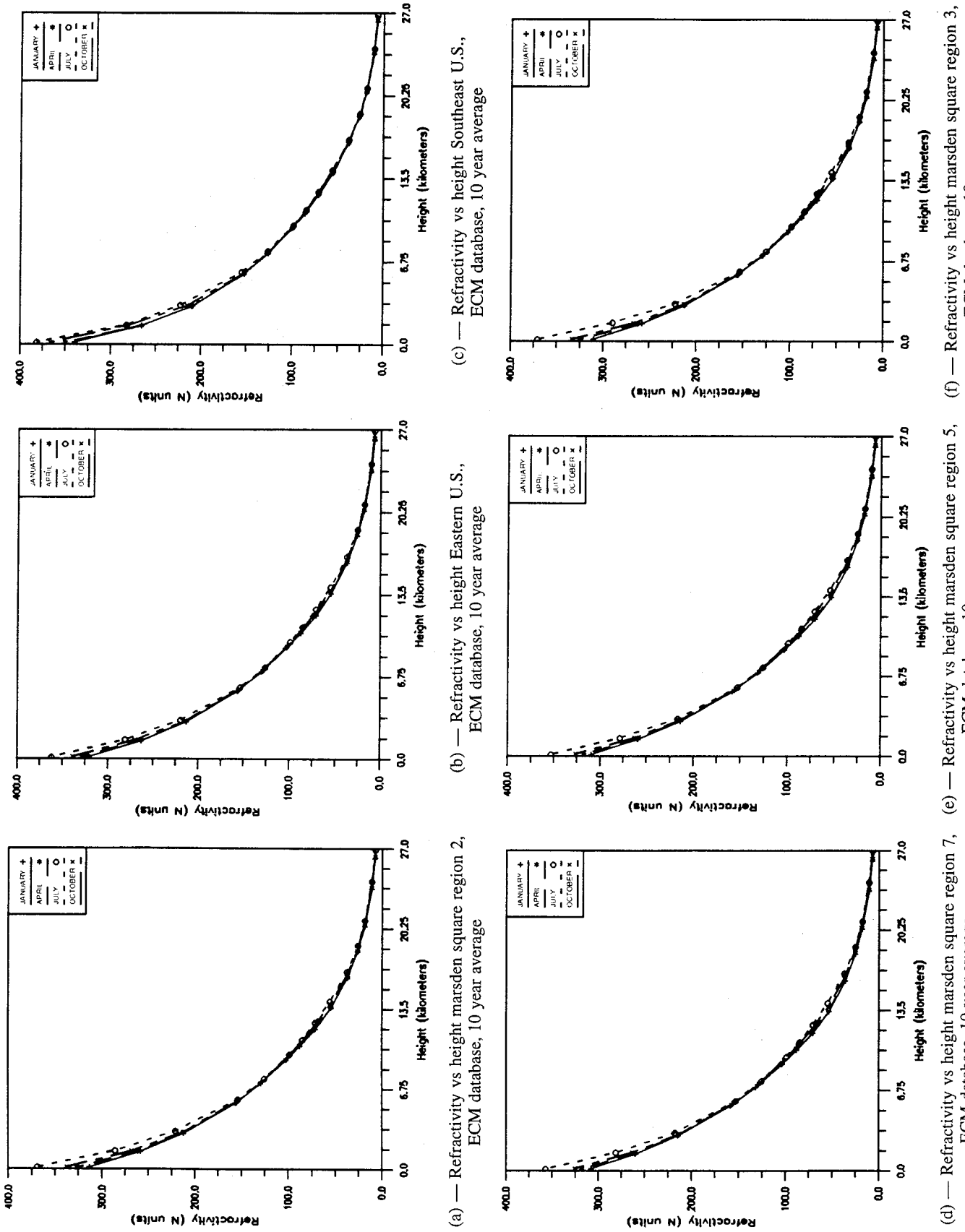

(a) — Refractivity vs height marsden square region 2, ECM database, 10 year average

(b) — Refractivity vs height Eastern U.S., ECM database, 10 year average

(c) — Refractivity vs height Southeast U.S., ECM database, 10 year average

(d) — Refractivity vs height marsden square region 7, ECM database, 10 year average

(e) — Refractivity vs height marsden square region 5, ECM database, 10 year average

(f) — Refractivity vs height marsden square region 3, ECM database, 10 year average

Fig. 5 — Refractivity vs height in Eastern U.S. by marsden square: (a) Mid-Atlantic coastal region, (b) Eastern areas—60 grids areas, (c) Florida peninsula and neighboring coast, (d) North Midwest—major part of Great Lakes, (e) Northeast—New England coastal area, and (f) Mideast region from Georgia to Ohio.

exponential function of height than a linear function as assumed by the effective Earth's radius model. The exponential decrease of N with height is sufficiently regular as to permit a first approximation of average N-unit structure from surface conditions alone [1]. Consider that,

$$N(h) = N_S \exp(-h/H) \tag{22}$$

where H is a scale or reference height appropriate to the value of N at zero height (or surface), N_S-surface refractivity and h the height above the mean surface level in kilometer [km]. Average values of N_S and H for the United States are approximately 313 and 7 km respectively. H varies regionally. For example, H is 7.3529 km for the global average and 10.0 km for the British Isles. However, climatic and synoptic changes in refractive index profiles can be accounted for by using the refraction variables of the surface ranging from 220, extremely dry and high locations, to 450, extremely hot and humid locations. Refraction effects are also more sensitive to initial N-gradient conditions than to the value of N_S, particularly at small elevation angles below 5°. It is also noted that the scale height varies along with variations of the surface refractivity of the local region. Many different models [1, 2] had been proposed similar to Eq. (22), and thus will not be presented here.

Figure 6 shows monthly variations of refractivity over 12 months period for different portions of Eastern U.S. All graphs are within latitude 32.5° to 47.5° N and longitude 65° to 90° W, and are divided by a 2.5° × 2.5° grid increment to distinguish from each other features such as mountain, ocean, and coastline areas. It is noticed that refractivities of all localized areas are similar below 500 mbar level or 5.7 km above the mean-sea-level (MSL). This implies that atmospheric activities in the troposphere are mainly below 10 km above MSL.

The second order gradients of monthly refractivities, delta N1 – delta N2, for each different region in the Eastern U.S. are shown in Figs. 7 and 8 to investigate the dynamic behavior of lower atmospheres (less than 3 km high above the surface). The delta N1 represents the first order gradient of refractivities between the surface's refractivities and the refractivities at 1.5 km above the surface where the pressure level is approximately 850 mbar. The delta N2 is the next layer's first-order gradient of refractivities between 850 mbar level (1.5 km high above the surface) and 700 mbar level (3 km high above the surface). Finally, delta (N1 – N2) gradient represents the difference between delta N1 and delta N2.

The particular bar-graphs of Figs. 7 and 8 describe the dynamic profiles of each regional atmosphere from January to December over 10 year period. The coastal region (CST) covers (latitude 32.5° to 47.5° N and longitude 65° to 80° W), ocean region (OCN) between (latitude 32.5° to 45° N and longitude 65° to 77.5° W) marsden square region 1 through 4 (MS 1 through MS 4) covers (latitude 32.5° to 42.5° N and longitude 65° to 90° W) by keeping latitude constant and shifting longitude 5° W from MS1 (marsden square 1, longitude 65° to 75° W) to MS 4 (marsden square 4, longitude 80° to 90° W). Likewise, marsden square 5 through 8 (MS 5 through MS 8) covers (latitude 37.5° to 47.5° N and longitude 65° to 90° W) by fixing latitude and shifting longitude by 5° increment from MS 5 (marsden square 5, longitude 65° to 75° W) to MS 8 (marsden square 8, longitude 80° to 90° W). Finally, SE 2 (Southeastern U.S., latitude 22.5° to 32.5° N and longitude 85° to 95° W) region covers most of the Gulf Coast of the Florida panhandle and SE 3 (Southeastern U.S., latitude 22.5° to 32.5° N and longitude 75° to 85° W) covers most of the Florida peninsula with more than 50% being ocean areas. As noticed from the bar-graphs, refractivity gradient for inland areas such as marsden square 5 through 8 are smaller than coastal regions such as CST, OCN, MS 2, MS 3, SE2 and SE3.

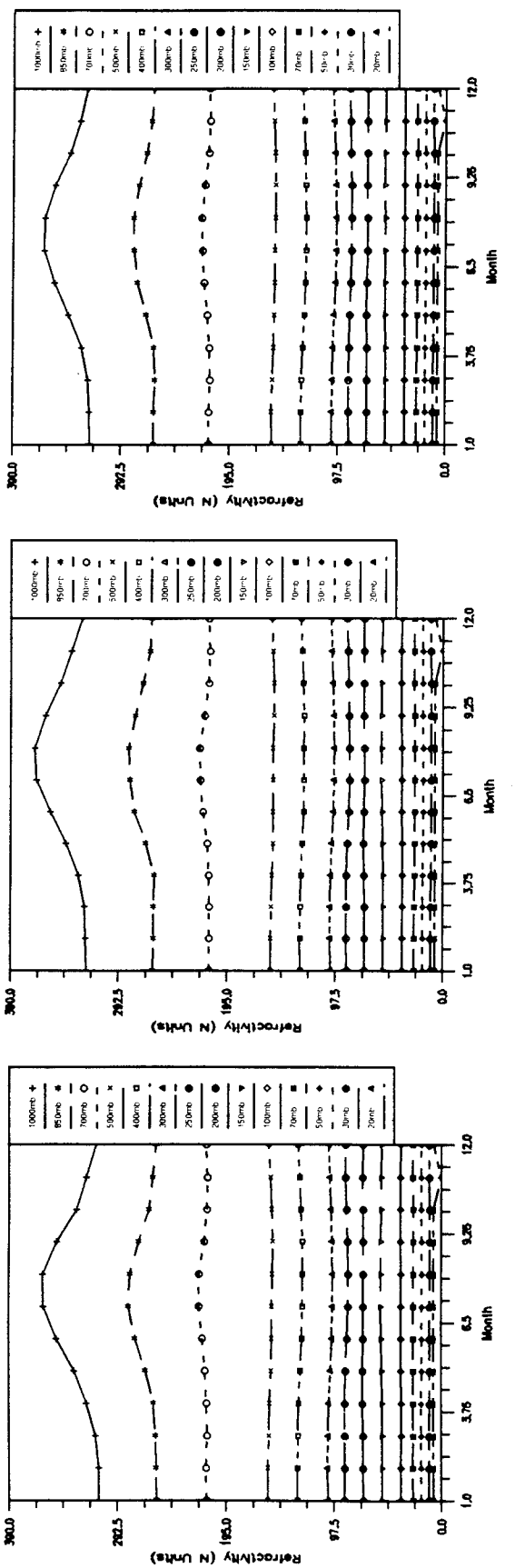

(a) — Refractivity vs month coast, ECM database, 10 year average with respect to pressure level

(b) — Refractivity vs month ocean, ECM database, 10 year average with respect to pressure level

(c) — Refractivity vs month Eastern U.S., ECM database, 10 year average with respect to pressure level

(d) — Refractivity vs month marsden square 2, ECM database, 10 year average with respect to pressure level

(e) — Refractivity vs month inland, ECM database, 10 year average with respect to pressure level

(f) — Refractivity vs month mountain, ECM database, 10 year average with respect to pressure level

Fig. 6 — Monthly mean refractivity variations: (a) Atlantic Coast, (b) Atlantic Ocean close to Eastern U.S., (c) Eastern U.S., (d) mid-Atlantic coastal area, (e) Mideast of U.S., and (f) Appalachian mountain areas

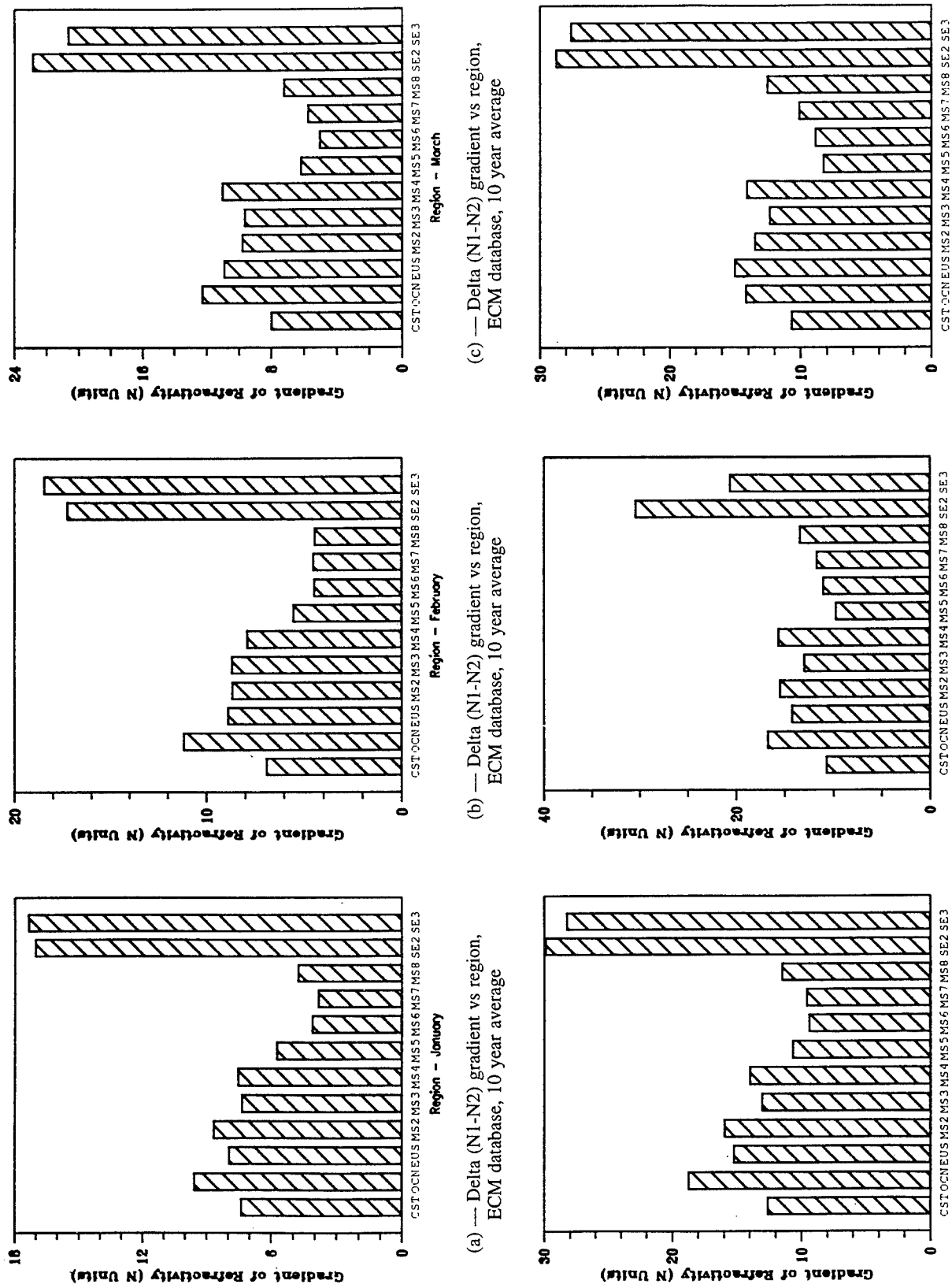

(a) — Delta (N1-N2) gradient vs region, ECM database, 10 year average

(b) — Delta (N1-N2) gradient vs region, ECM database, 10 year average

(c) — Delta (N1-N2) gradient vs region, ECM database, 10 year average

(d) — Delta (N1-N2) gradient vs region, ECM database, 10 year average

(e) — Delta (N1-N2) gradient vs region, ECM database, 10 year average

(f) — Delta (N1-N2) gradient vs region, ECM database, 10 year average

Fig. 7 — Second-order refractivity gradient for Eastern U.S. region by partitioned local areas from January to June over the period of 1980-1991: (a) January, (b) February, (c) March, (d) April, (e) May, and (f) June.

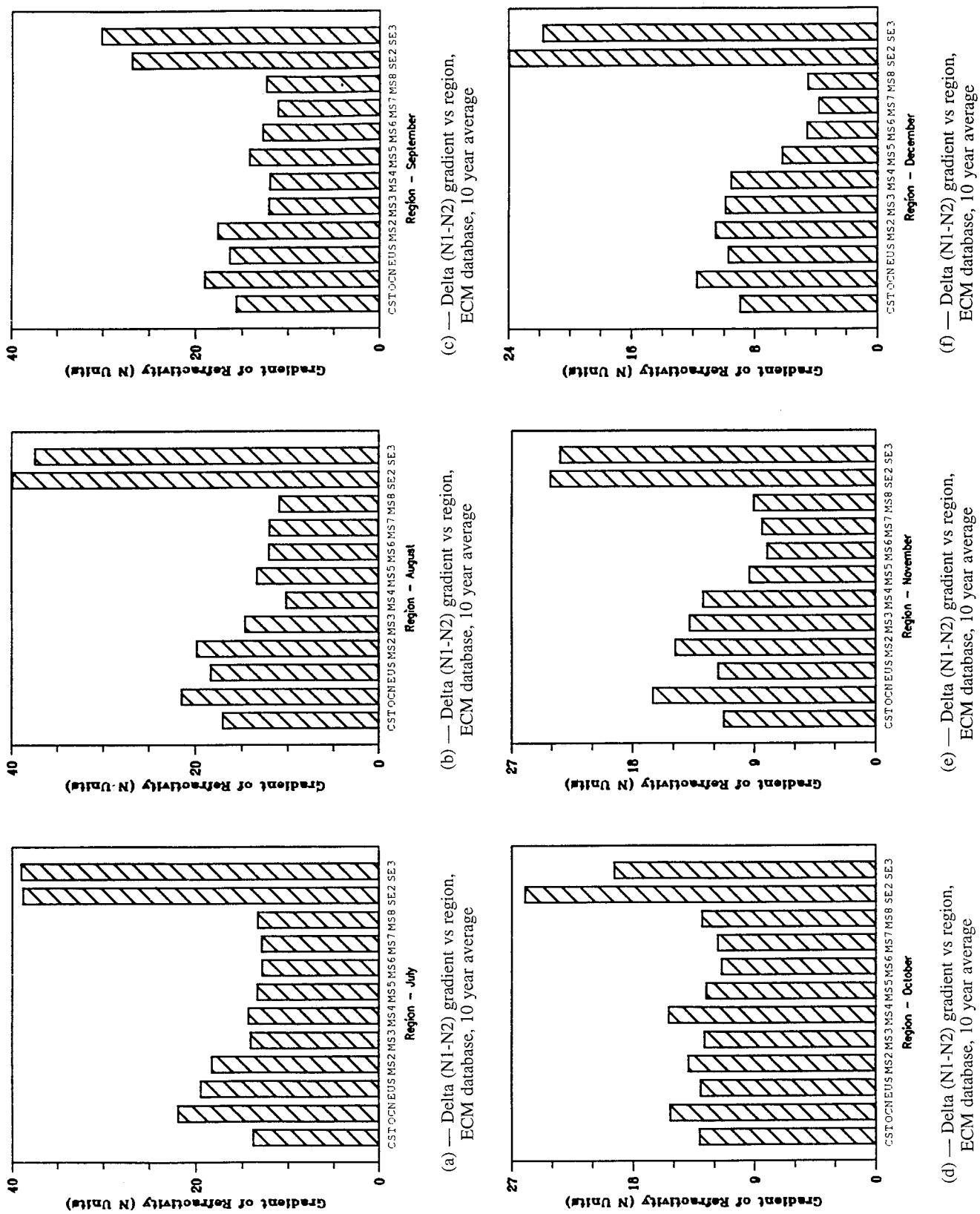

(a) — Delta (N1-N2) gradient vs region, ECM database, 10 year average

(b) — Delta (N1-N2) gradient vs region, ECM database, 10 year average

(c) — Delta (N1-N2) gradient vs region, ECM database, 10 year average

(d) — Delta (N1-N2) gradient vs region, ECM database, 10 year average

(e) — Delta (N1-N2) gradient vs region, ECM database, 10 year average

(f) — Delta (N1-N2) gradient vs region, ECM database, 10 year average

Fig. 8 — Second-order refractivity gradient for Eastern U.S. region by partitioned local areas from July to December over the period of 1980-1991: (a) July, (b) August, (c) September, (d) October, (e) November, and (f) December.

RANGE ERRORS

Signal deterioration is caused by the existence in the atmosphere of spatial inhomogeneities that are continuously varying as a function of time. The spatial variations generally produce statistical bias errors, while the time-varying component results in the fluctuating or root-mean-square inaccuracies. The propagational effects that are prevalent when radio waves traverse the atmosphere manifest themselves as refractive bending, time delays, Doppler errors, rotation of the plane of polarization (Faraday Effect), dispersion effects, and attenuation. The atmospheric radio refraction effects in the troposphere cause an extra time delay in transmission of the signal, and an increase in the elevation angle measured by the antenna system. In other words, there are two types of errors: errors in measuring distance by means of timing the transit of radio signals between two points, known as range errors, and errors in estimating the elevation angle of a target by means of measuring the angle of arrival of radio signals from the target or spacecraft, known as elevation angle errors.

Many methods have been proposed to take into account these refraction effects for the purpose of improving measurements by removing systematic bias [21, 22, 23]. For the case of range error, this error is composed of two parts: the difference between the curved length of the ray path R, and the true slant range R_0 mainly due to the increase in time necessary to travel over the curved path R; and the discrepancy caused by the lowered velocity of propagation in a refractive medium as shown in Fig. 9. The radio ray path R can be expressed by, [4]

$$R = \int_0 n \csc \theta \, dh \tag{23}$$

where

- n represents the refractive index,
- θ the elevation angle,
- csc stands for cosecant angle of trigonometry, and
- h the height above the surface.

Then the total range error ΔR can be computed by

$$\begin{aligned} \Delta R &= R - R_0 \\ &= \int_0 n \csc \theta \, dh - R_0 . \end{aligned} \tag{24}$$

Many of the range models are based on the following assumptions of ray tracing:

a. The refractive index should not change appreciably in a wavelength.
b. The fractional change in the spacing between neighboring rays (initially parallel) must be small in a wavelength.

Note also that the Eqs. (23) and (24) are derived with the assumption of a flat Earth. For a flat Earth, the attenuation as a function of elevation angle is given by the zenith attenuation multiplied by the cosecant of the elevation angle. The cosecant law does not hold for elevation angles less than 6° to 10° due to Earth curvature and refraction effects. Most satellite communication systems operate at elevation angles above 6° or a cosecant of 10° [24]. Barton and Ward in [25] proposed approximate range and elevation angle errors as follows,

$$\Delta R = 0.007\ N_s \csc \theta_o \quad \text{[meters]} \tag{25}$$

$$\Delta\theta_o = N_s \cot \theta_o \quad \text{[}\mu\text{radian]} \tag{26}$$

where

- N_s is surface refractivity, and
- θ_o the apparent elevation angle.

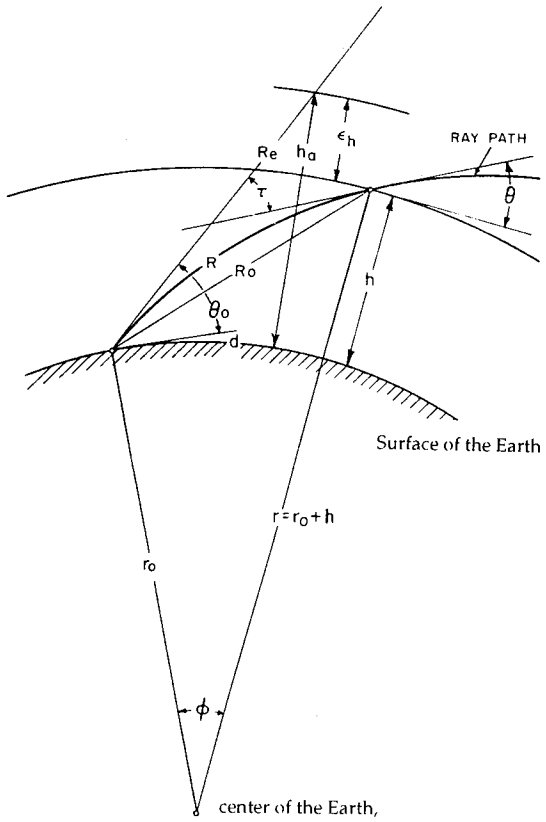

Fig. 9 — Radiowave propagation geometry of radio ray refraction

The conclusion can be construed that for targets that lie well outside the troposphere, the errors in range and elevation angle are seen to level off at values that depend upon elevation angle but not on range. Many other models for range and angle error have been proposed over the years [2, 7, 8, 20, 21]. These models are generally developed from either a direct integral method or a stratified layer method, either of which can be applied to compute the angular deviation and range inaccuracy introduced when electromagnetic waves traverse a medium other than free space. The latter method, although only approximate in nature, is capable of rendering theoretical estimates of proportional errors to a rather high degree of accuracy, and it is presented here by adopting Millman's approach in [6] without extensive derivation efforts. Also, note that most of the ray-tracing plots presented in this report used the stratified layer method. Considering Eq. (23) by parameters,

$$dh = dr/\sin\theta \tag{27}$$

$$\sin\theta = [1 - (n_o r_o \cos\theta_o/nr)^2]^{1/2} \tag{28}$$

where

- r_o is the radius of the Earth,
- n_o the refractive index at the Earth's surface as shown in Fig. 9.

Then the range error can be written as

$$R = (1/n_o r_o \cos\theta_o) \int n^2 r \, dr/[\,(nr/n_o r_o \cos\theta_o)^2 - 1]^{1/2}. \tag{29}$$

When we further look into the characteristics of Eq. (29), the denominator inside the integral Eq. (29) is going to be zero for low elevation angles. If the elevation angle θ_o is less than 1°, Eq. (29) is not integrable since n approaches to n_o when h approaches zero. Thus, the integral has a singularity when h goes to zero in the limit, i.e, over the horizon. In other words, Eq. (29) is valid if and only if the elevation angle is greater than one degree or higher.

Using the trigonometric functions in Fig. 9, R_o can be easily derived as

$$R_o = [r_o^2 + (r_o + h)^2 - 2r_o(r_o + h)\cos\theta]^{1/2} \tag{30}$$

where θ is the central angle subtended over the Earth's surface. Therefore, the range error of Eq. (24) is readily derived by substituting Eqs. (29) and (30). For the stratified layer approach, Eqs. (29) and (30) can be rewritten in discrete format as in Eqs. (31), (32), and (33) below by numerical approximation methods such as Gauss's and Simpson's rules for numerical approximation of integral equations. The graphical representation of the stratified layer approach is shown in Fig. 10. The range error ΔR of Eq. (24) may be approximated as

$$\Delta R = \Sigma n_j R_j - R_{om}. \tag{31}$$

Similarly, Eqs. (29) and (30) can be approximated as:

$$R_j^2 = r_j^2 + r_{j+1}^2 - 2r_j r_{j+1}\cos\theta_j \tag{32}$$

$$R_{om}^2 = r_o^2 + r_{m+1}^2 - 2\, r_o\, r_{m+1}\cos[\Sigma\,\theta_j] \tag{33}$$

where r_o is the Earth's radius at the station and m represents the *m*th layer.

Figure 11 was plotted for comparison purposes among regional range error behavior against elevation angle variations over four seasonal activities in the Eastern U.S. areas by using Eqs. (31-33). Figure 11(a) covers the Great Lakes areas by season. Figure 11(b) covers the Northeast region mainly in the mid-Atlantic coast with latitude 37.5° to 47.5° N and longitude 65° to 75° W. Figure 11(c) covers mid-Atlantic inland areas with latitude 22.5° to 32.5° N and longitude 75° to 85° W. Figure 11(d) covers mid-Atlantic coastal region with latitude 32.5° to 42.5° N and longitude 70.0° to 80.0°W. Figure 11(e) covers the entire Eastern U.S. region with latitude 22.5° to 52.5° N and longitude 65.0° to 100.0° W, and Fig. 11(f) shows Southeast U.S. areas with latitude 22.5° to 32.5° N and longitude 75.0° to 105.0° W for Florida peninsula and surrounding coastal areas. As shown in

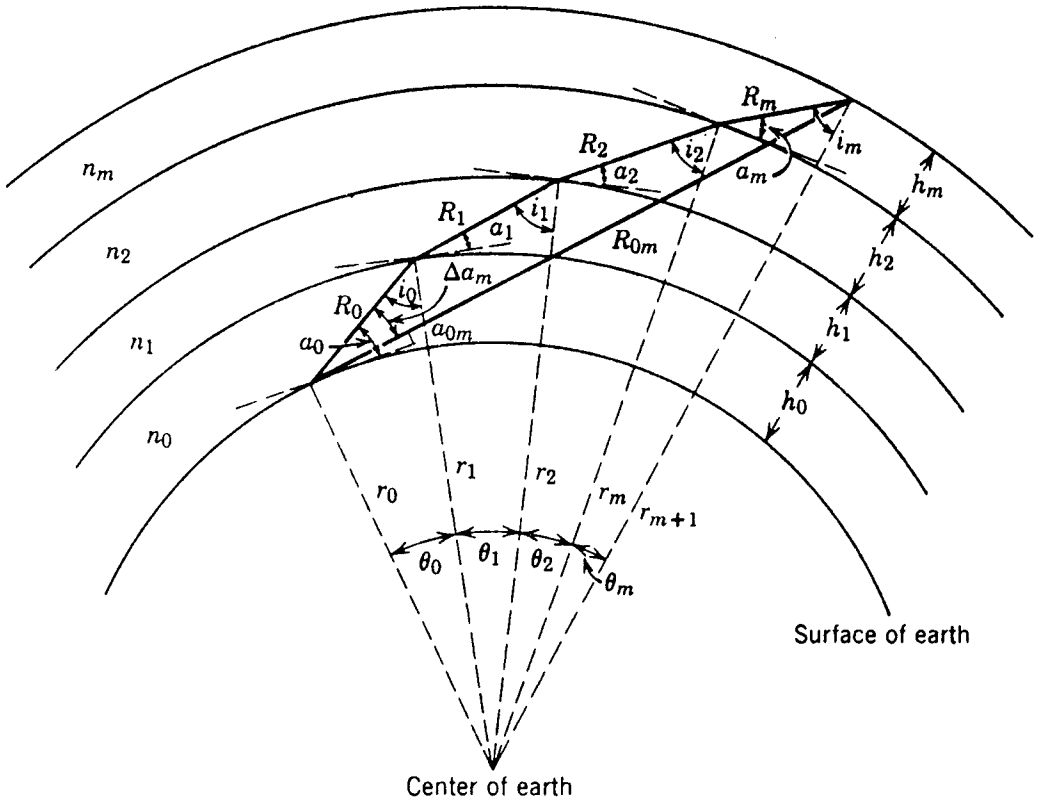

Fig. 10 — Progressive bending of a ray traversing spherical atmospheric lay stratification

the Fig. 11, range error variations of all four seasons do not vary significantly while Fig. 11(c) and 11(f) show more variations in July activities.

Figure 12 presents seasonal plots of range errors vs height variation for three Eastern U.S. coastal region from New England to Florida's Key West with three elevation angles of 1°, 3°, and 5°, marsden square 5 covers the area of latitude 37.5° to 47.5° N and longitude 65° to 75° W, marsden square 2 with latitude 32.5° to 42.5° N and longitude 70° to 80° W, and Southeast U.S. 3 with latitude 22.5° to 32.5° N and longitude 75° to 85° W. As shown in Fig. 12(c), range error variations in July are rather higher and dynamic in comparison with those in January (Fig. 12(a)) and April (Fig. 12(b)) months. It is noticed that range error variations in the month of October in Fig. 12(d) are slightly larger than those in January and April since there may be more humidity in the fall season. It is also noticed that range errors of 1° elevation angle are above 80 m and are much higher than 20 m and 40 m of the 3° and 5° elevation angles respectively. This implies that range errors of 1° elevation angle can increase up to twice the range errors of the 3° elevation angles.

Figure 13 shows range error plots with elevation angles from 1° to 15° for four seasons in the Eastern U.S. region. As expected, variations of range error of wider coverage areas are rather smooth in comparison with local regions of grid level (2.5° × 2.5°) or marsden square level (10.0° × 10.0°). Range errors for the lower elevation angles for 1.0° are around 80 m for July and 70 m for the month of January, while those for the 5.5° elevation angle are about 27 m for July and about 25 m for January. This implies that range errors at 5.5° elevation angle are reduced by 65% less than those at 1.0° elevation angle. If this is converted to time delay, it will be a minimum of 76 ns for January, the month when refractivity is generally lower than that of the other months of the year. If we increase the elevation angle to 15°, then the range errors are about 7.8 m for July and 7.7 m for

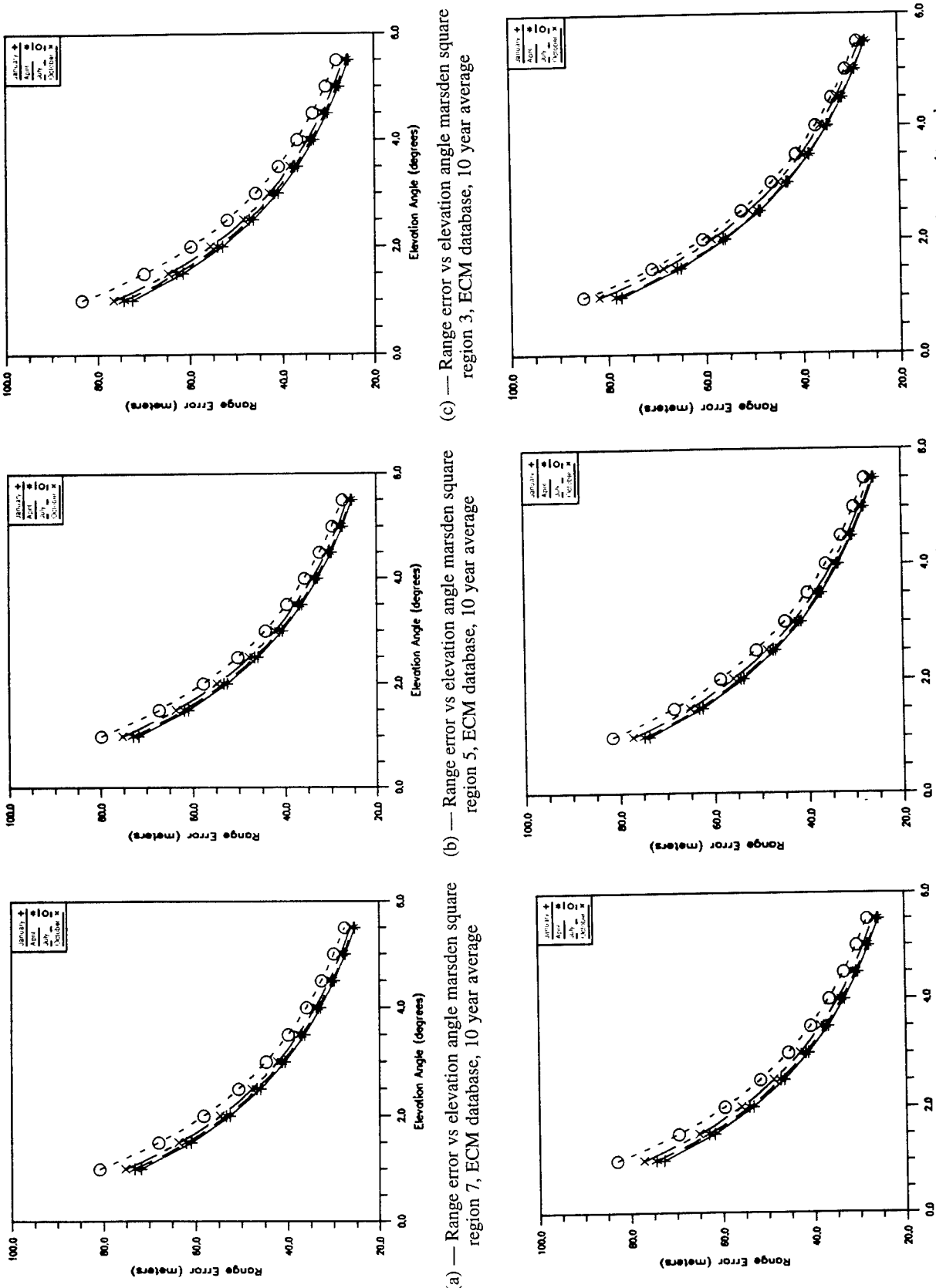

(a) — Range error vs elevation angle marsden square region 7, ECM database, 10 year average

(b) — Range error vs elevation angle marsden square region 5, ECM database, 10 year average

(c) — Range error vs elevation angle marsden square region 3, ECM database, 10 year average

(d) — Range error vs elevation angle marsden square region 2, ECM database, 10 year average

(e) — Range error vs elevation angle East U.S., ECM database, 10 year average

(f) — Range error vs elevation angle Southeast U.S. region 3, ECM database, 10 year average

Fig. 11 — Range error vs elevation angle from 1° to 5.5°: (a) Great Lakes region, (b) Northeast coastal region, (c) Mideast inland region including Appalachian mountain areas, (d) mid-Atlantic coast, (e) Eastern U.S., and (f) Southeast U.S. from Florida to Eastern Texas.

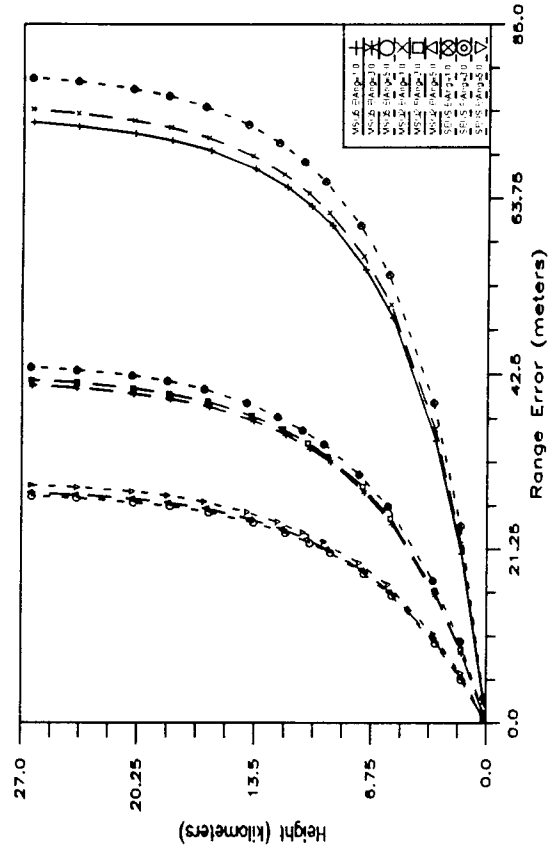

(a) — Range error vs height, MSQ5, MSQ2, Southeast U.S., ECM database, January, 10 year average

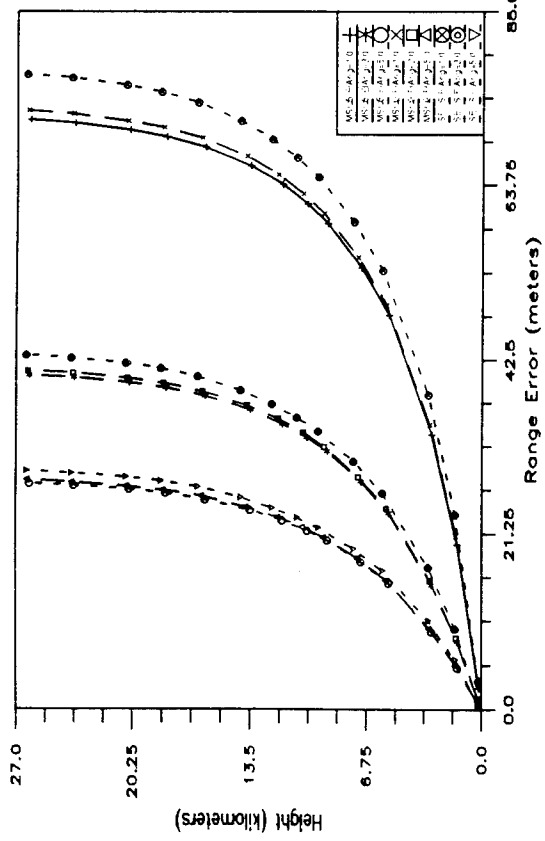

(b) — Range error vs height, MSQ5, MSQ2, Southeast U.S., ECM database, April, 10 year average

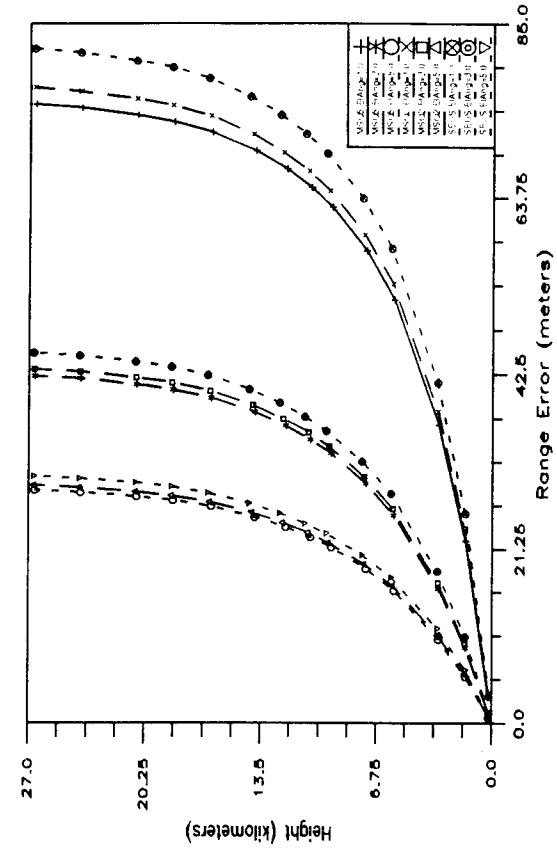

(c) — Range error vs height, MSQ5, MSQ2, Southeast U.S., ECM database, July, 10 year average

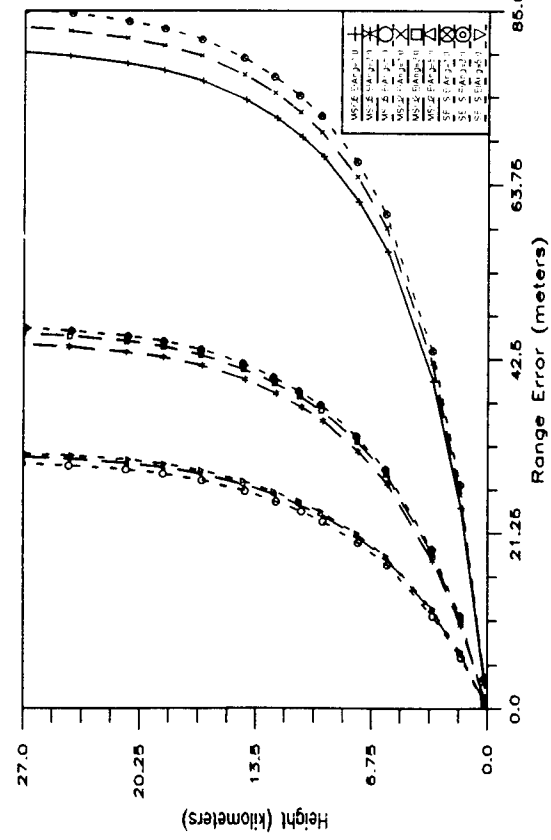

(d) — Range error vs height, MSQ5, MSQ2, Southeast U.S., ECM database, October, 10 year average

Fig. 12 — Range error vs height from 1° to 5.5° elevation angle over the Eastern U.S. coast: (a) January, (b) April, (c) July, and (d) October.

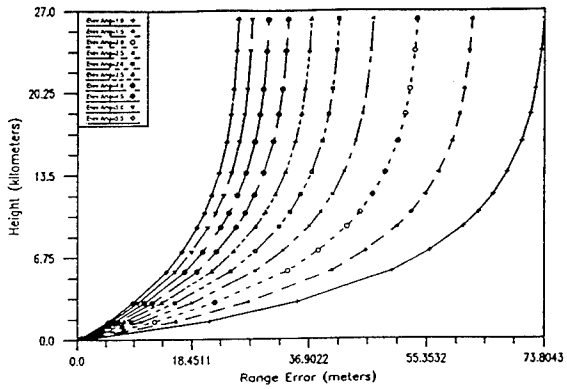

(a) Height vs range error U.S., January (1° to 5.5°)

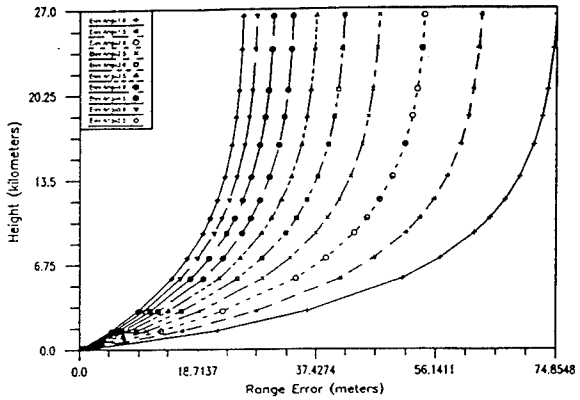

(b) Height vs range error U.S., April (1° to 5.5°)

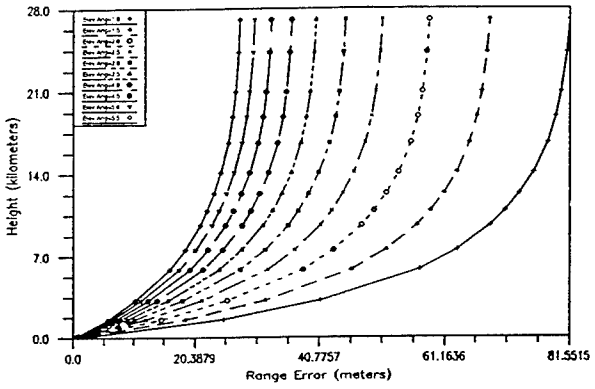

(c) Height vs range error U.S., July (1° to 5.5°)

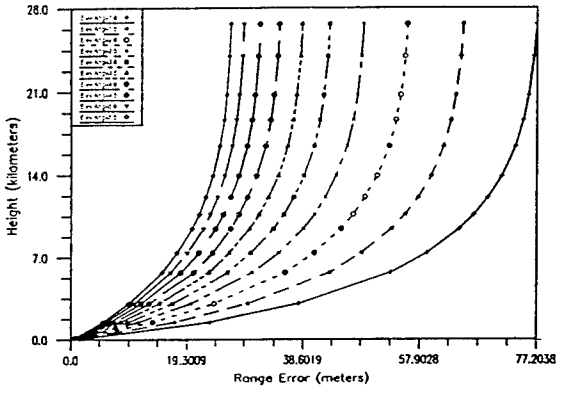

(d) Height vs range error U.S., October (1° to 5.5°)

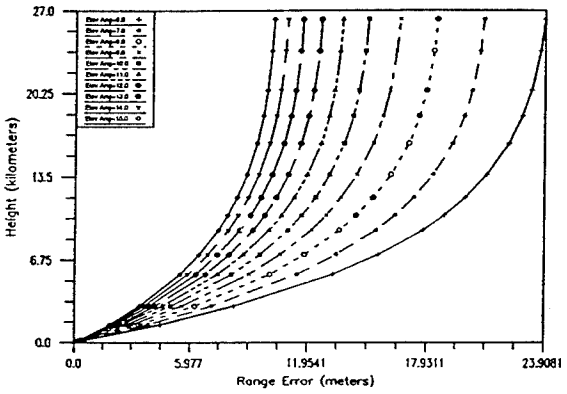

(e) Height vs range error U.S., January (6° to 15°)

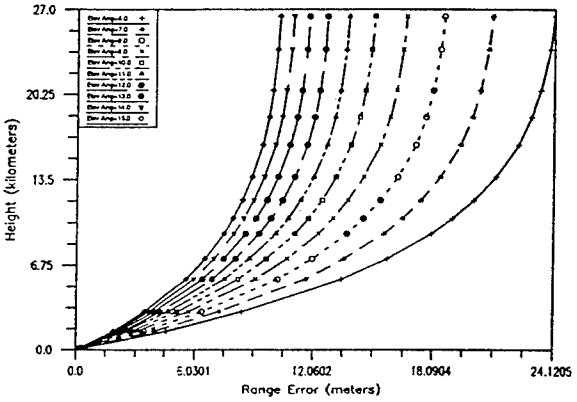

(f) Height vs range error U.S., April (6° to 15°)

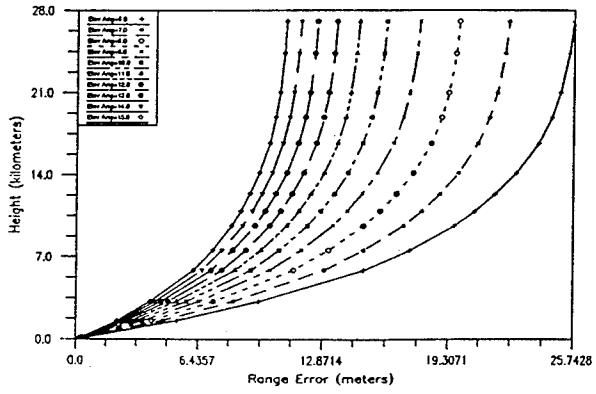

(g) Height vs range error U.S., July (6° to 15°)

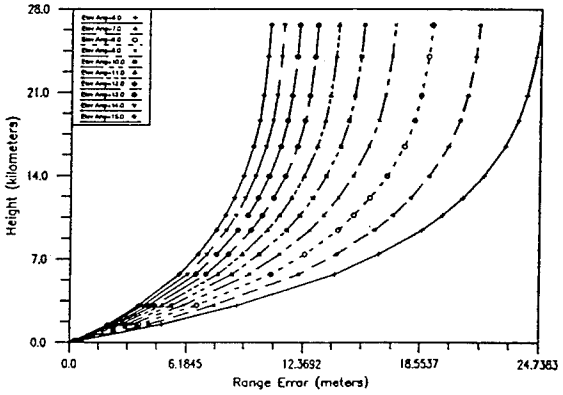

(h) Height vs range error U.S., October (6° to 15°)

Fig. 13 — Height vs range error from 1° to 15° elevation angle over entire Eastern U.S. for four seasons: (a)-(d) for 1° to 5.5°, and (e)-(h) for 6° to 15° from January to October, respectively.

January. This means that range errors at 15° elevation angle are reduced 10% less than those at a range error of 1.0° elevation angle. Finally, it is noticed that range errors vary seasonally as well as monthly from few m to about 10 m range in the low elevation angles.

ELEVATION ANGLE ERRORS

The index of refraction varies from day to day and even from hour to hour in the troposphere. These large scale irregularities that are usually found at height levels of approximately 1 and up to 10 km are influenced, to a large extent, by the weather and season. Under these conditions, the refractivity may vary as much as 20 N-units within a height interval of only 30 to 100 m. In addition to the large-scale irregularities, small-scale variations in the refractive index have been observed by means of microwave refractometer techniques [4]. The standard fluctuation deviation in the refractivity, which is presumably the result of atmospheric turbulence, is usually on the order of 0.25° to 0.3° N-units. Since the atmospheric bending of electromagnetic waves is mostly dependent on the refractive index profile along the path traveled by the waves, random variations of this parameter will necessarily produce a continuous fluctuation in the angular position of a radar target. Variations in tropospheric refraction give rise to changes in the angle of arrival of radio waves amounting rarely to more than a small fraction of a degree. Measurements of the angle of arrival may be checked with expectations based on observed index of refraction profiles.

As already pointed out, the angular error is caused by the ray bending of the radar beam such that the wavefront reflected from a target appears to be coming from a direction other than the target's true angular position in space. Errors in elevation angle are mainly caused by the refractive effects. The fluctuations are generally higher in summer, which is consistent with the increase in surface refractivity that normally occurs in this period. Corrections can be made for errors in the angle of arrival . These corrections are most useful if they are based on standard or mean models of the radio refractive index such that surface values can be used as a predictor. A successful method of deriving such a model is found in ray tracing through a representative sample of refractive index profiles (or refractivity profiles) and relating refraction variables to surface values using least square techniques. Ordinarily, a linear relationship is sufficient with the coefficients being functions of the elevation angle and target height or range. Since the surface value of the refractive index is so central to refraction prediction, a detailed examination of its behavior is essential.

For a vertical gradient of refractive index dn/dh, the radius of curvature ρ is given by, [26]

$$1/\rho = -(1/n) \times (dn/dh) \times \cos \theta_o \tag{34}$$

where θ_o is the initial elevation angle of the ray at the transmitter with respect to the local horizon as shown in Fig. 9. The negative sign indicates a decrease in refractive index with height. For terrestrial propagation, where θ_o is generally close to zero, the Eq. (34) simplifies to

$$1/\rho = -dn/dh \tag{35}$$

with n assumed to be unity in Eq. (34). As can be seen in Eqs. (34) and (35), the curvature or the bending is due to the refractive index changes. Refractive index is relatively insensitive to frequency. One thing to note is that the assumption of n = 1 in Eq. (35) is not true in the troposphere from the ground surface to about 30 km into space. In general, the value n is greater than one by the Eqs. (16) or (17) depending on the value of refractivity at the layers concerned. A relationship between the elevation angle error (or ray bending) and surface refractivity N_s has been developed [4] for low elevations through a statistical linear regression technique giving

$$\Delta\theta = (bN_s + a) * 10^{-6} \text{ radians} \tag{36}$$

where the coefficients a and b are provided through graphics or tables [4]. Equation (36) does not apply to regions of climatic extremes, or for angles less than 3° or 4°. For example, eastern regions of semipermanent subtropical high pressure areas such as Dakar, Senegal, Southern California and the coast of South West Africa, the Arabian Gulf area and the parts of the monsoon region in India and Pakistan, as well as Arctic locations can be cited as typical areas of interests [27]. For the limiting errors of targets well beyond the atmosphere where $\theta > 5°$,

$$\Delta\theta \approx N_s \cot\theta * 10^{-6} \text{ radians.} \tag{37}$$

Many other ray-tracing models have been proposed to improve the accuracy of atmospheric bending or propagation delay [2, 4]. The stratified ray-tracing model has been applied in this report with other integral methods since it gives better result than other approaches tested [7, 8].

If it is assumed that the refractive index is a function only of height above the surface of a smooth, spherical Earth (i.e., it is assumed that the refractive index structure is horizontally homogeneous) and that the refractive index is a monotonically decreasing function of altitude, then the path of a radiowave ray will obey the Snell's law for polar coordinates (Bouger's Rule) as:

$$n_1 r_1 \cos\theta_1 = n_2 r_2 \cos\theta_2 \tag{38}$$

where n is the radio refractive index of the atmosphere, r is the radial distance from the center of the Earth to the point under consideration, and θ is the elevation angle made by the ray at the point under consideration with the tangent to the circle of radius r passing through that point as defined in Fig. 10. One should keep in mind that Eq. (38) is subject to the following restrictions of ray tracing as pointed out in the previous section:

1. The refractive index should not change appreciably in a wavelength (there is no discontinuity in the refractive index or gradient of refractive index, which is negligibly small).
2. The fractional change in the spacing between neighboring rays (initially parallel) must be small in a wavelength (basic requirement from Fermat's principle for geometrical optics).

Angle errors can alternatively be expressed in terms of the bending angle τ (as defined in Fig. 9) which is the change of the apparent angle of elevation with altitude by using Snell's law.

$$\tau = -\int (dn/n) \cot\theta^a - \int \cot\theta \, dN * 10^{-6} \tag{39}$$

where the integral limit spans from n1 to n2 for the refractive index of the first integral and from N1 to N2 for the refractivity of the second integral in Eq. (39).

Applying the law of sines and Eq. (40) below with a reference to Fig. 10, it follows that the elevation angle error can generally be derived for the stratified approach as, [6]

$$\alpha_{om} = \cos^{-1}\{(r_{m+1}/R_{om}) \sin[\Sigma_j \theta_j]\}. \tag{40}$$

Then the refraction elevation angle error can be expressed as

$$\Delta\alpha_m = \alpha_o - \alpha_{om} \tag{41}$$

where α_o is the apparent elevation angle and α_{om} is the true elevation angle.

Many other expressions for elevation angle error have been proposed since the late 1950's including Bean & Dutton in [4], Bertram in [28], Rowlandson & Moldt in [23], Black in [8], Hopfield in [2], Goad in [7], in Blake [3], etc. Those derivations are not presented in this report to avoid any complexity or confusion. References are provided at the end of the report for those who are further interested in the subject.

Figure 14 shows the ray-tracing graph depicting elevation angle vs atmospheric height from the ground for the marsden square 7 which covers most of the Great Lakes area. Elevation angles extend from 1.0° to 5.5°. Elevation angle errors are of the largest numbers in July, while the second largest number occurs in October, and the smallest in January. It is noticed that all angle errors in this low elevation angle range exceed 1 mrad (0.0573°) and extend to more than 6 mrad in the summer.

Figure 15 shows angle errors vs atmospheric height from 6° to 15° of elevation angle for the marsden square 7. Angle errors are of the largest amount in July, and the second largest occurs in October, the smallest amount occurs in January as expected. From these ray-tracing plots, it is noticed that elevation angle errors are significant, up to 10° elevation angle if one would like to maintain the angle error within 1 mrad throughout the entire year.

Figure 16 shows three regional ray-tracing graphs from New England to the Florida peninsula during the four season from 1° to 5.5° of apparent elevation angles. As in Figs. 14 and 15, elevation angle errors are of the largest amount in July with the second largest in October and the smallest in January. In general, elevation angle errors are higher in the Florida peninsula region than in both mid-Atlantic and New England areas throughout the year.

Finally, the relationship between apparent elevation angle and the corresponding elevation angle error is shown in Fig. 17. The amount of angle error varies by season and locality as shown in Fig. 17. Marsden square region 2 (latitude 32.5° to 42.5° N and longitude 70° to 80° W) and marsden square region 3 (latitude 32.5° to 42.5° N and longitude 75.0° to 85.0° W) show higher angle errors than other local areas during the month of July. Elevation angle errors of marsden square regions 5, 7 and the Atlantic coastal region in the month of July are lower than those for the entire Eastern U.S. regional average in the month of July. Other seasons show to be very close to each other for these local regions including the entire Eastern U.S. region. This implies that some local areas generate larger angle errors than much larger regional averages. This is also true for the global average data. It should be noted that elevation angle errors in radiowave propagation vary dynamically throughout the season and regional areas specifically in the low elevation angle. One should be cautious in correcting radiowave beam bending and propagation delay when applying global climatological data to radiowave propagation for radar tracking and antenna pointing applications.

CORRELATION ANALYSIS OF METEOROLOGICAL PARAMETRIC VARIABLES

The main purpose here is to study correlational phenomena of refractivity variations in the atmosphere among meteorological parameters. Correlation analysis enables us to detect whether there is any connection among certain measurements, and if so, what the connections represent. It

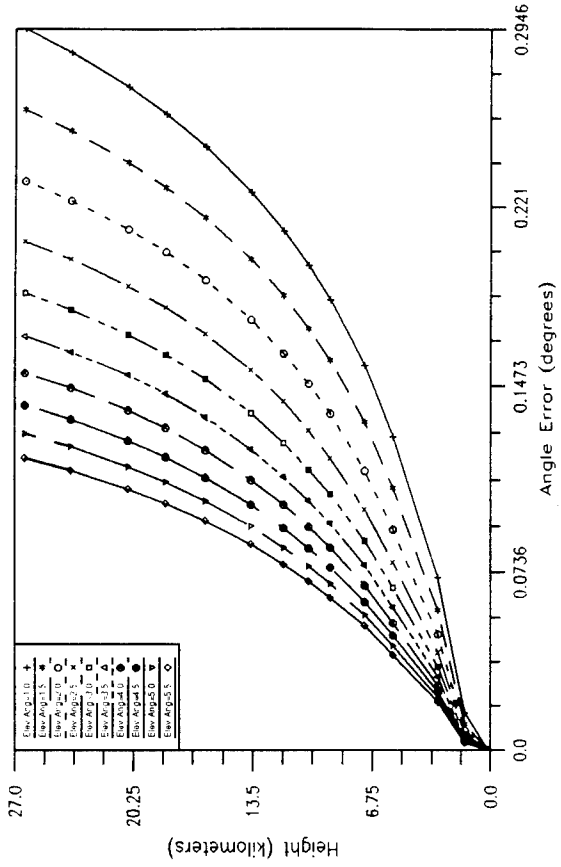

(a) — Height vs angle error marsden square region 7, ECM database, 10 year average, January

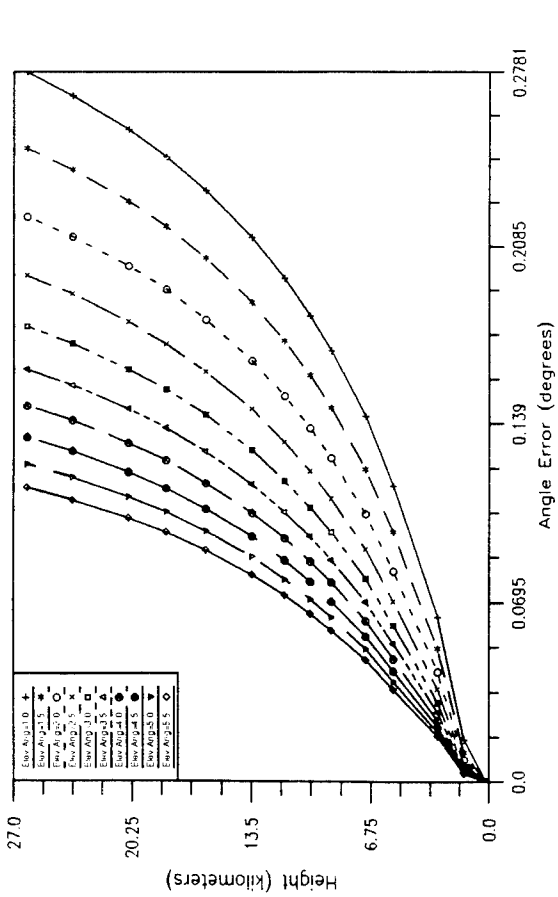

(b) — Height vs angle error marsden square region 7, ECM database, 10 year average, April

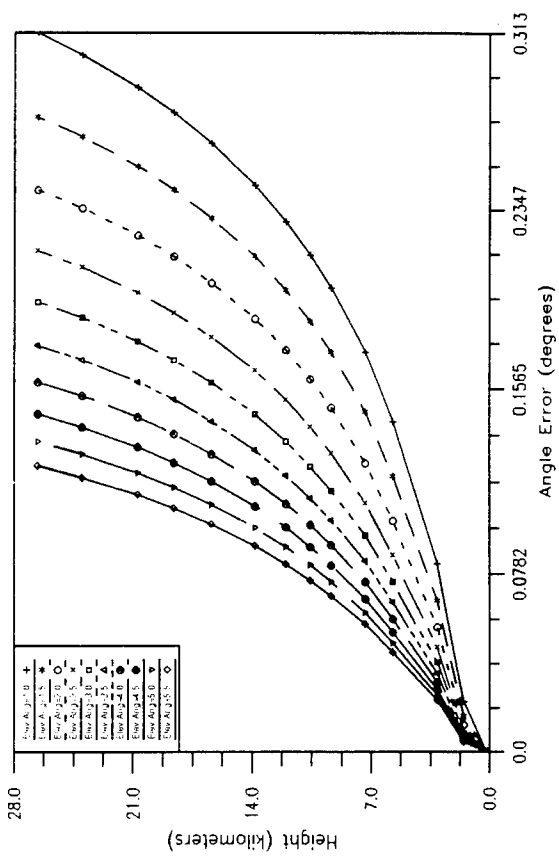

(d) — Height vs angle error marsden square region 7, ECM database, 10 year average, October

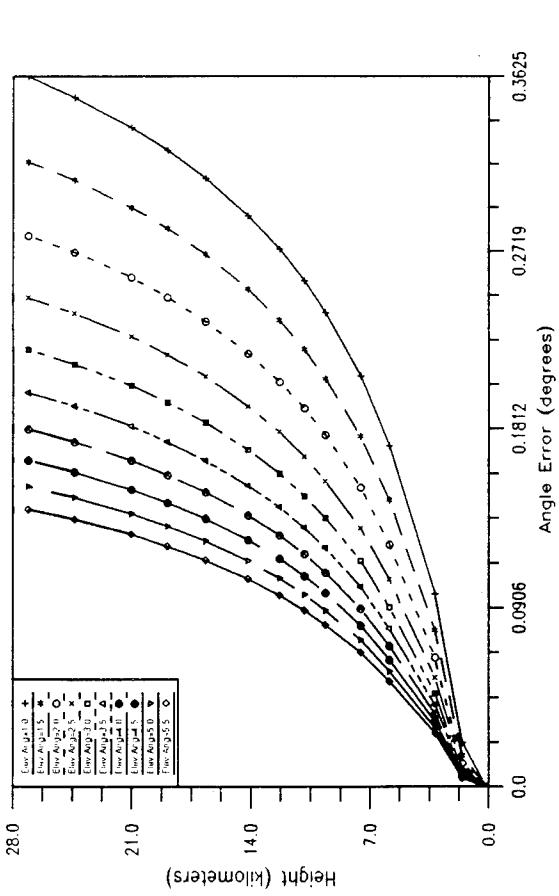

(c) — Height vs angle error marsden square region 7, ECM database, 10 year average, July

Fig. 14 — Elevation angle error vs height from 1° to 5.5° over marsden square 7 (latitude 37.5° to 47.5° N and longitude 75° to 85° W) for the four seasons

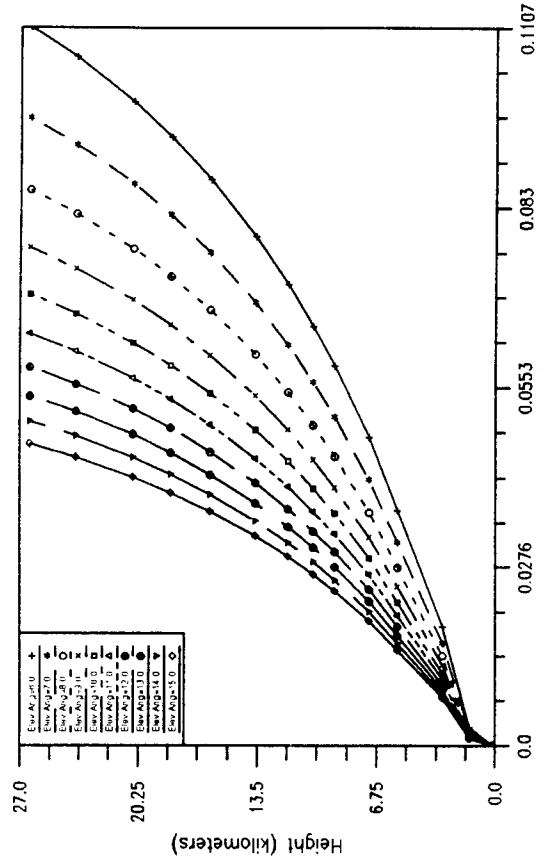

(a) — Height vs angle error, marsden square region 7, ECM database, 10 year average, January

(b) — Height vs angle error, marsden square region 7, ECM database, 10 year average, April

(c) — Height vs angle error, marsden square region 7, ECM database, 10 year average, July

(d) — Height vs angle error, marsden square region 7, ECM database, 10 year average, October

Fig. 15 — Elevation angle error vs height from 6° to 15° over marsden square 7 (latitude 37.5° to 47.5° N and longitude 75° to 85° W)

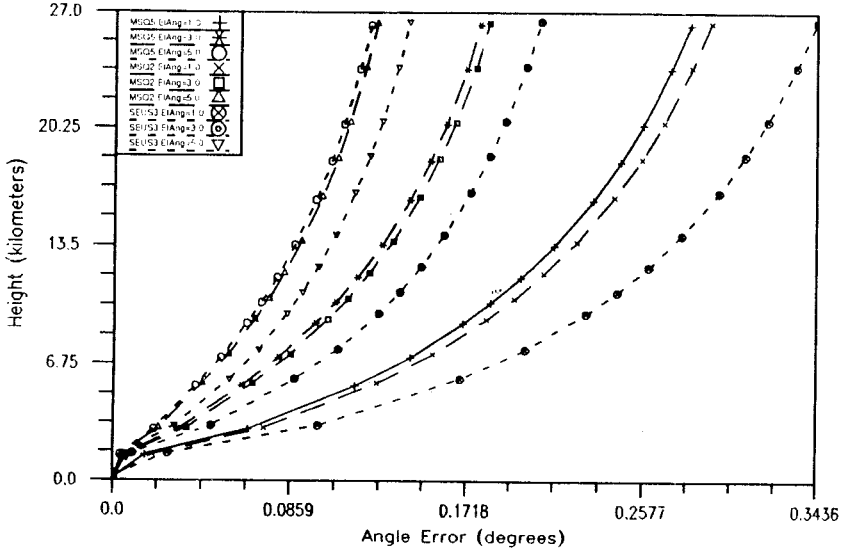

(a) — Height vs angle error, MSQR5, MSQR2, SEUS3, ECM data, 10 year average, January

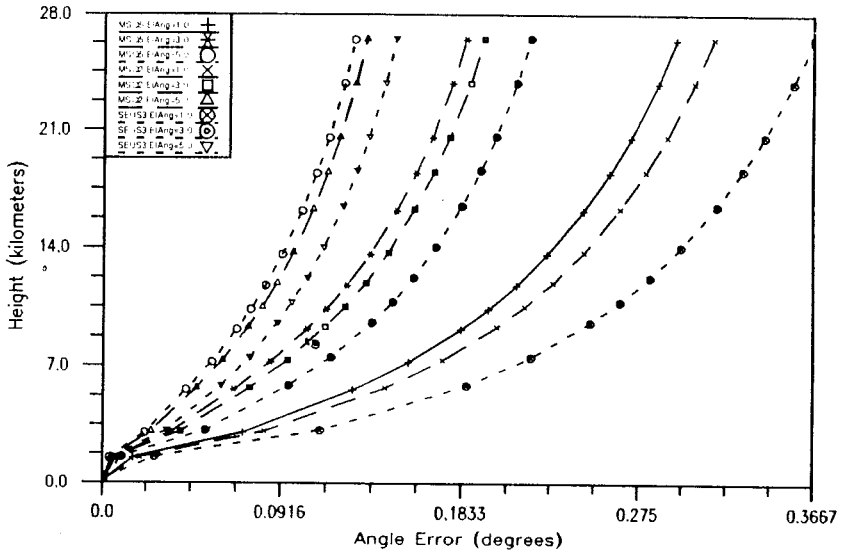

(b) — Height vs angle error, MSQR5, MSQR2, SEUS3, ECM data, 10 year average, April

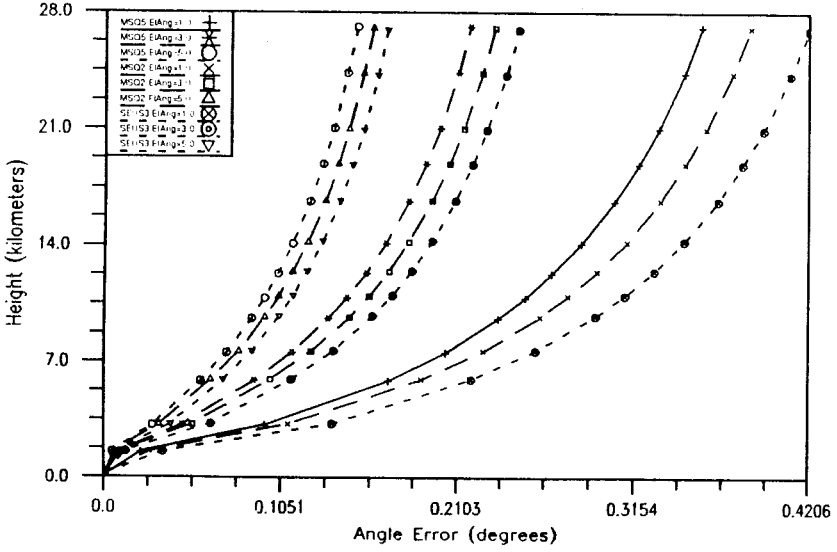

(c) — Height vs angle error, MSQR5, MSQR2, SEUS3, ECM data, 10 year average, July

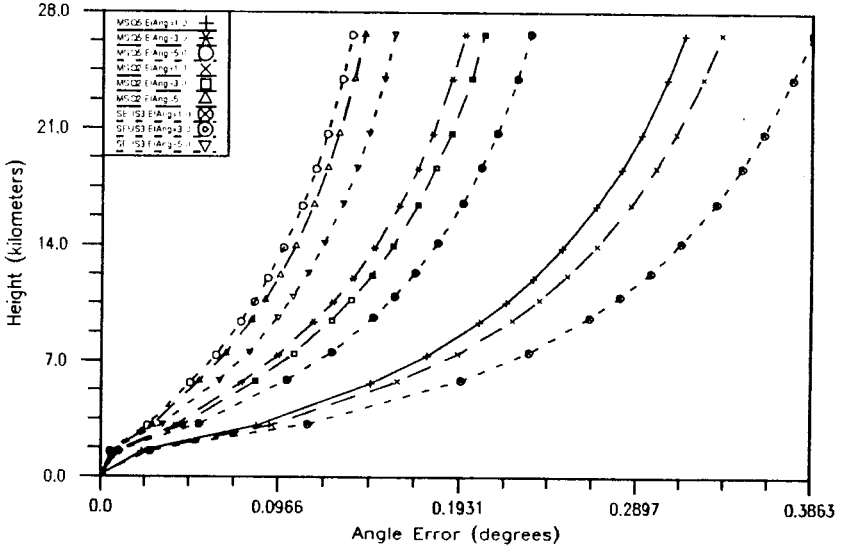

(d) — Height vs angle error, MSQR5, MSQR2, SEUS3, ECM data, 10 year average, October

Fig. 16 — Elevation angle error vs height from 1°, 3°, and 5° over marsden square 5 (latitude 37.5° to 47.5° N and longitude 65° to 75° W) and marsden square 2 (latitude 32.5° to 42.5° N and longitude 70° to 80° W) for the four seasons

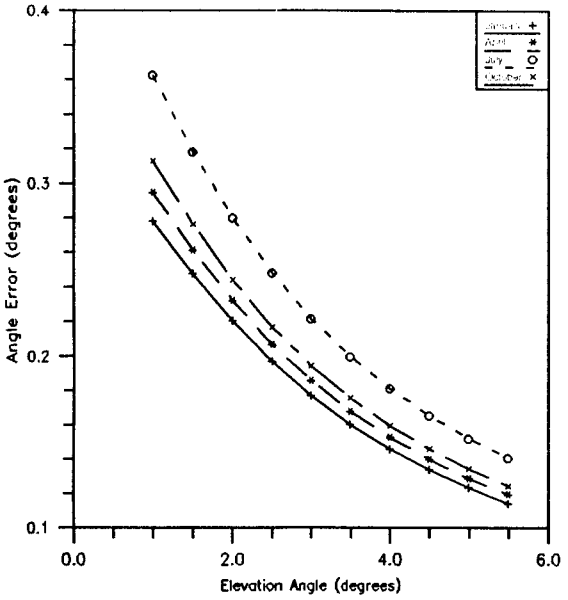

(a) — Angle error vs elevation angle, marsden square region 7, ECM database, 1° to 5.5°, 10 year average

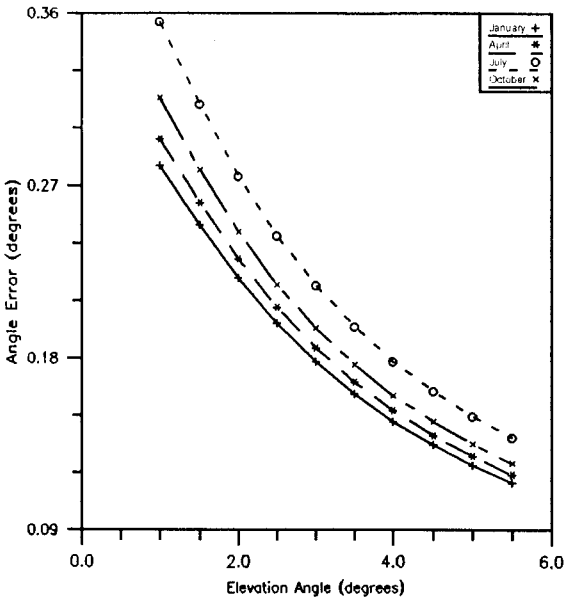

(b) — Angle error vs elevation angle, marsden square region 5, ECM database, 1° to 5.5°, 10 year average

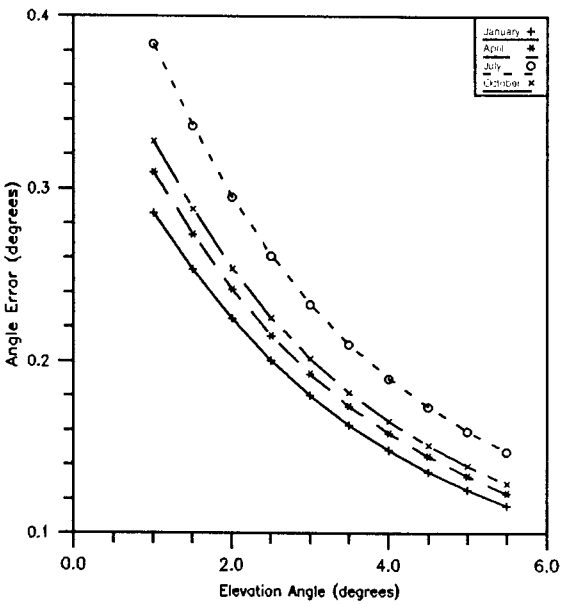

(c) — Angle error vs elevation angle, marsden square region 3, ECM database, 1° to 5.5°, 10 year average

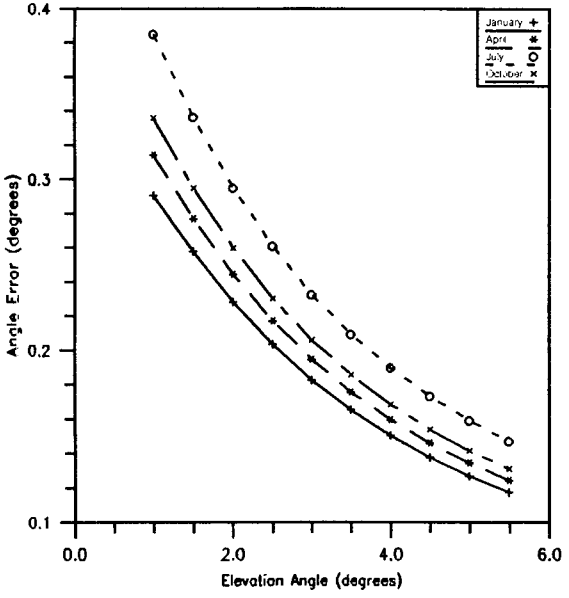

(d) — Angle error vs elevation angle, marsden square region 2, ECM database, 1° to 5.5°, 10 year average

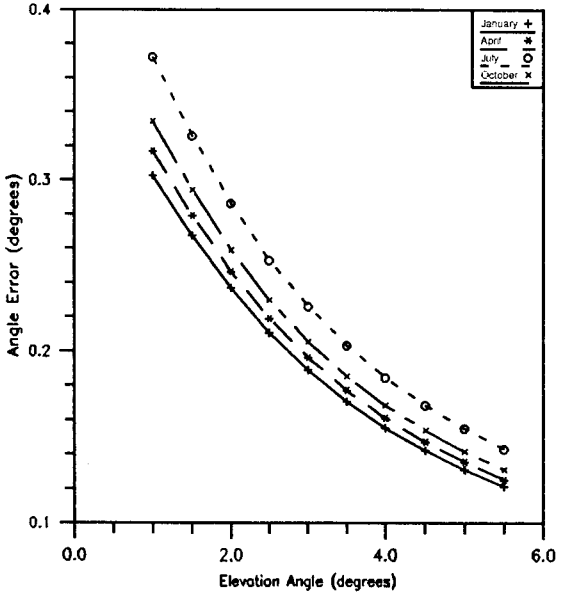

(e) — Angle error vs elevation angle, Eastern U.S., ECM database, 1° to 5.5°, 10 year average

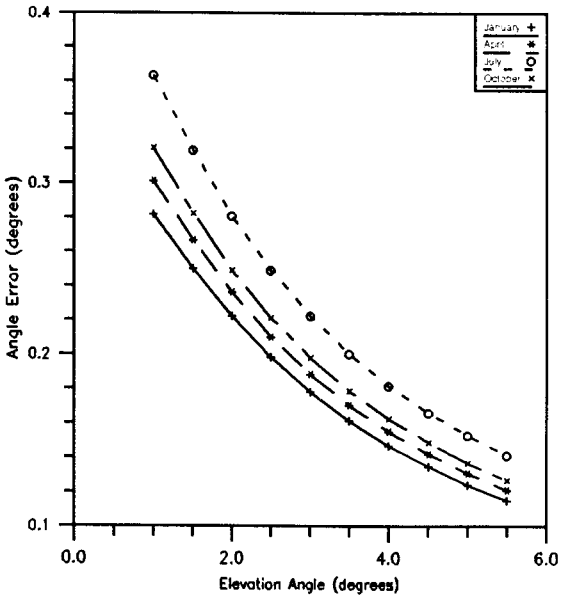

(f) — Angle error vs elevation angle, coastline, ECM database, 1° to 5.5°, 10 year average

Fig. 17— Elevation angle error vs elevation angle from 1° to 5.5° over marsden square 2, 3, 5, and 7, Eastern U.S. and Atlantic coast for four seasons

establishes whether a series of measurements or a period of time of observation are two measurement values independent of one another, or whether covariation or contravariation exist between them. Here, correlation analysis abandons its original purpose of establishing functional relationships between parameters and leads instead to a probable new concept for characterizing ray bending and the angle of arrival prediction in the radio frequency propagation through space.

Variations in the radio refractive index are both a nuisance and a blessing in a manner similar to the discussion of aerosols and hydrometers. For some systems (e.g., microwave distance measuring equipment), radio refractive index fluctuations are environmentally noisy and must be eliminated in the processed signal. For other systems, such as the FM-CW radar and other clear air radars, refractive index fluctuations are indicative of atmospheric structure and are often used to trace phenomena much larger than the scale of the fluctuations [1]. Should be noted that a high degree of accuracy of temperature, pressure, and water vapor pressure measurements is essential and necessary for a precise determination of the refractivity, Eq. (18). If one assumes that the formula for N is exact, then a relation between small changes in temperature, pressure, and water vapor pressure may be evaluated from [4]

$$dN = (\partial N/\partial T)\, dT + (\partial N/\partial e)\, de + (\partial N/\partial P)\, dP \tag{42}$$

assuming that the errors in P, T, and e are not related. In Eq. (42), the first term of the partial derivatives is the relation between refractivities and temperature; similarly, the second term represents the relation between refractivity and water vapor pressure, which can be transferred into relative humidity by Eq. (16). Finally, the third term of the Eq. (42) gives the relation between refractivity and pressure. These relational analyses will be shown later in this section with other parameter relational analyses. Equation (42) can also be very useful in determining the control level accuracies that would be required to achieve a certain overall accuracy of refractive index in the laboratory calibration of refractometers. The partial derivatives may be evaluated by reference to some standard atmosphere to yield the approximate expression as

$$\Delta N' = a\,\Delta T + b\,\Delta e + c\,\Delta P \tag{43}$$

where a, b, and c are values for U.S. Standard Atmosphere surface conditions. Coefficients, a, b, and c are parameters describing relationships between refractivity vs temperature, relative humidity, and pressure, respectively.

The root mean square (rms) errors for some average atmospheric condition can then be written in finite difference form as

$$\Delta N = [(a\,\Delta T)^2 + (b\,\Delta e)^2 + (cDP)^2\,]^{1/2}. \tag{44}$$

As noted from Eq. (18), ΔN is quite sensitive to Δe and least sensitive to ΔP. Thus in moist regions (that include all but the most arid regions of the lower troposphere) fluctuations in N are caused by fluctuations in water vapor content. In relatively dry regions, such as the middle and upper troposphere, N fluctuations are indicative of temperature variations.

In addition to these errors, other sources of error may be evaluated such as refractivity vs range error or angle error. The first and second order gradient of refractivities for the lower atmospheric layers may also provide valuable information regarding dynamic variational behavior of local atmosphere by season or month. Time delay vs height variation and elevation angle vs propagation delay study are included for additional tropospheric phenomenon analysis. Many of these error

relational analyses are presented based on climatological data provided by ETAC (Environmental Technical Applications Center) at Scott Air Force Base.

Relational graphs have been plotted in Figs. 18, 19, and 20 for temperature, relative humidity, and pressure, respectively, to investigate phenomenal changes among these parameters from ground 0 to 27.0 km in space.

Figure 18 shows correlation phenomena between temperature and refractivity over marsden squares 2, 3, 5, 7 and Southeast U.S. region 3 with the entire Eastern U.S. region during four seasons. In the adiabatic layer, the relation between temperature variations and refractivity is very similar both seasonally, locally, and regionally. For the convection layer, there is sharp contrast relation between temperature and refractivity both seasonally and locally, as in Fig. 18(c), where temperature sharply increases, and in the rest of the graphs, where temperature increases rather smoothly except in Figs. 18(d) and 18(e).

Figure 19 shows the correlation activity between relative humidity and refractivity over marsden squares 2, 3, 5, 7 and Southeast U.S. region 3 (mainly Florida peninsula) with the entire Eastern U.S. region during the four seasons. Above 15 km in the atmosphere, where the refractivity is approximately 100° N-units, there is a minimal correlation between relative humidity and refractivity either in local or regional, coastal or inland, and warmer or cooler areas. In contrast with these phenomena, there are many good correlations between relative humidity and refractivity over the entire local and regional areas during the four seasons. It is noticeable that there is a more dynamic relation between relative humidity and refractivity over the Southeastern U.S.—Florida peninsula area in July, during the summer season.

Figure 20 shows the correlation between atmospheric pressure and refractivity over marsden squares 2, 3, 5, 7, and Southeast U.S. region 3 with the entire Eastern U.S. region for the four seasons. As expected, the results are almost identical among the graphs over the local and regional areas during the four seasons. This implies that atmospheric pressure is linearly proportional to the refractivity over local as well as larger regional areas and global.

Figures 21 through 23 show the relations between refractivity and elevation angle error for 1°, 5°, 10° apparent elevation angles over the four seasons in the six regional areas of the U.S. Figure 21(a) represents a functional correlation between refractivity and elevation angle error for the four seasons over Eastern U.S. (latitude 22.5° to 55.0° N and longitude 60.0° to 100.0° W); likewise Fig. 21(b) over western U.S. (latitude 22.5° to 55.0° N and longitude 100.0° to 135.0° W), Fig. 21(c) over Northeast U.S. (latitude 40.0° to 50.0° N and longitude 60.0° to 75.0° W), Fig. 21(d) over midwest U.S. (latitude 30.0° to 45.0° N and longitude 100.0° to 115.0° W), Fig. 21(e) over Alaska (latitude 45.0° to 60.0° N and longitude 170.0° W to 165.0° E), and Fig. 21(f) over Southeast U.S. (latitude 22.5° to 32.5° N and longitude 75.0° to 85.0° W). As noted in Fig. 21, Figs. 21(a), (c), and (e) have variable correlations between refractivity and elevation angle errors in comparison with Figs. 21(b), (d) and (f) that do not vary during the seasons. It is also noted that two distinct linear relations exist in the graphs, one from ground 0 to 3 km (about 700 mbar pressure level) in space, and the other from 3 km to 27.0 km in space, respectively. Figures 22 and 23 are similar for elevation angles 5° and 10°, respectively. It is noted that elevation angle errors for 1° apparent elevation angle are 5 to 7 mrad depending on the regions, while elevation angle errors for 10° apparent elevation angle are larger than 1 mrad around 18 km in space over the entire region in the U.S. during the four seasons. This result implies that tropospheric effects influence well over 5° elevation angles while most have argued until today that no tropospheric effects over 5° elevation angles are observed.

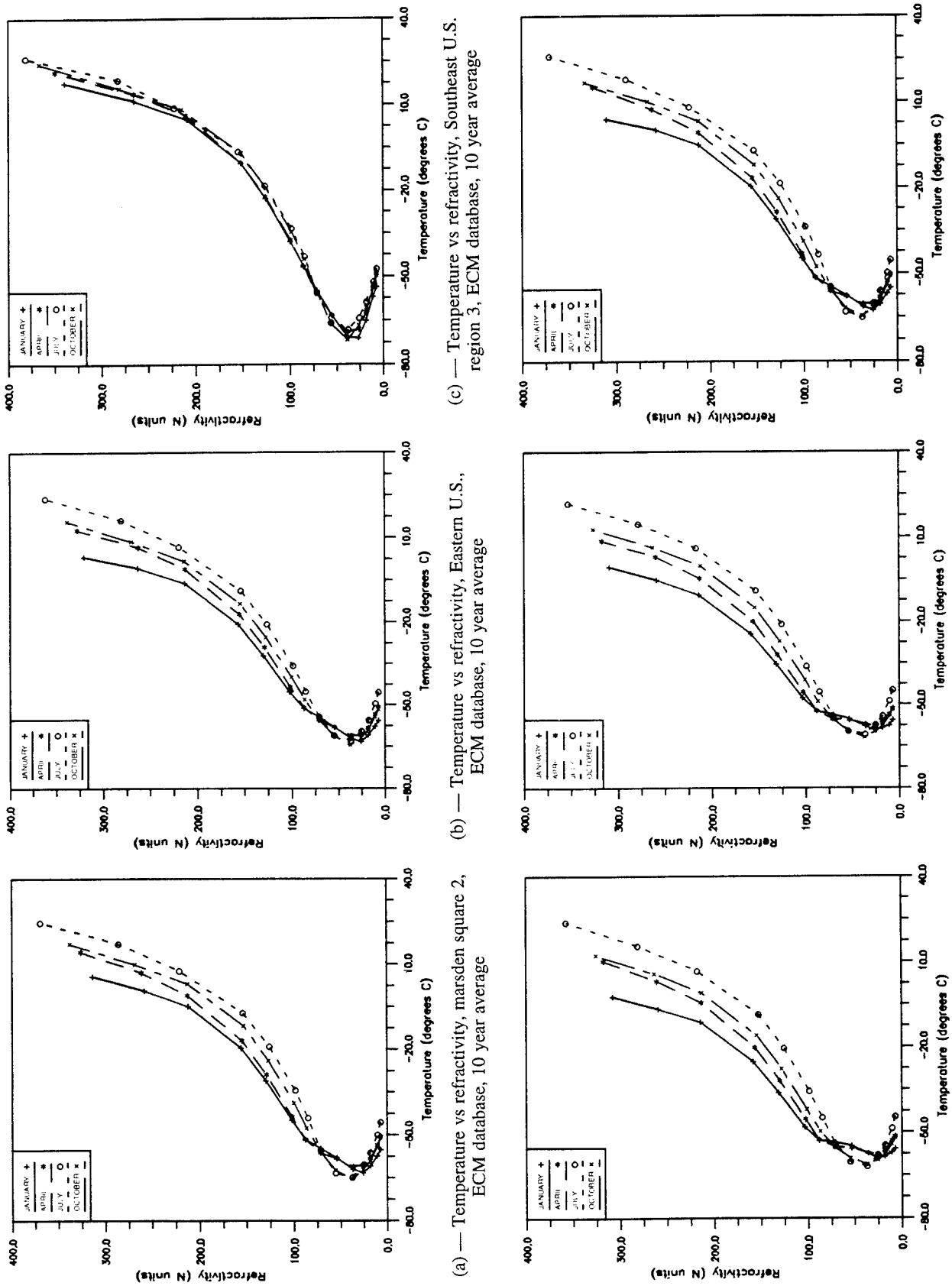

(a) — Temperature vs refractivity, marsden square 2, ECM database, 10 year average

(b) — Temperature vs refractivity, Eastern U.S., ECM database, 10 year average

(c) — Temperature vs refractivity, Southeast U.S. region 3, ECM database, 10 year average

(d) — Temperature vs refractivity, marsden square 7, ECM database, 10 year average

(e) — Temperature vs refractivity, marsden square 5, ECM database, 10 year average

(f) — Temperature vs refractivity, marsden square 3, ECM database, 10 year average

Fig. 18 — Seasonal temperature vs refractivity over marsden squares 2, 3, 5, and 7, Southeast U.S., region 3, and Eastern U.S. region

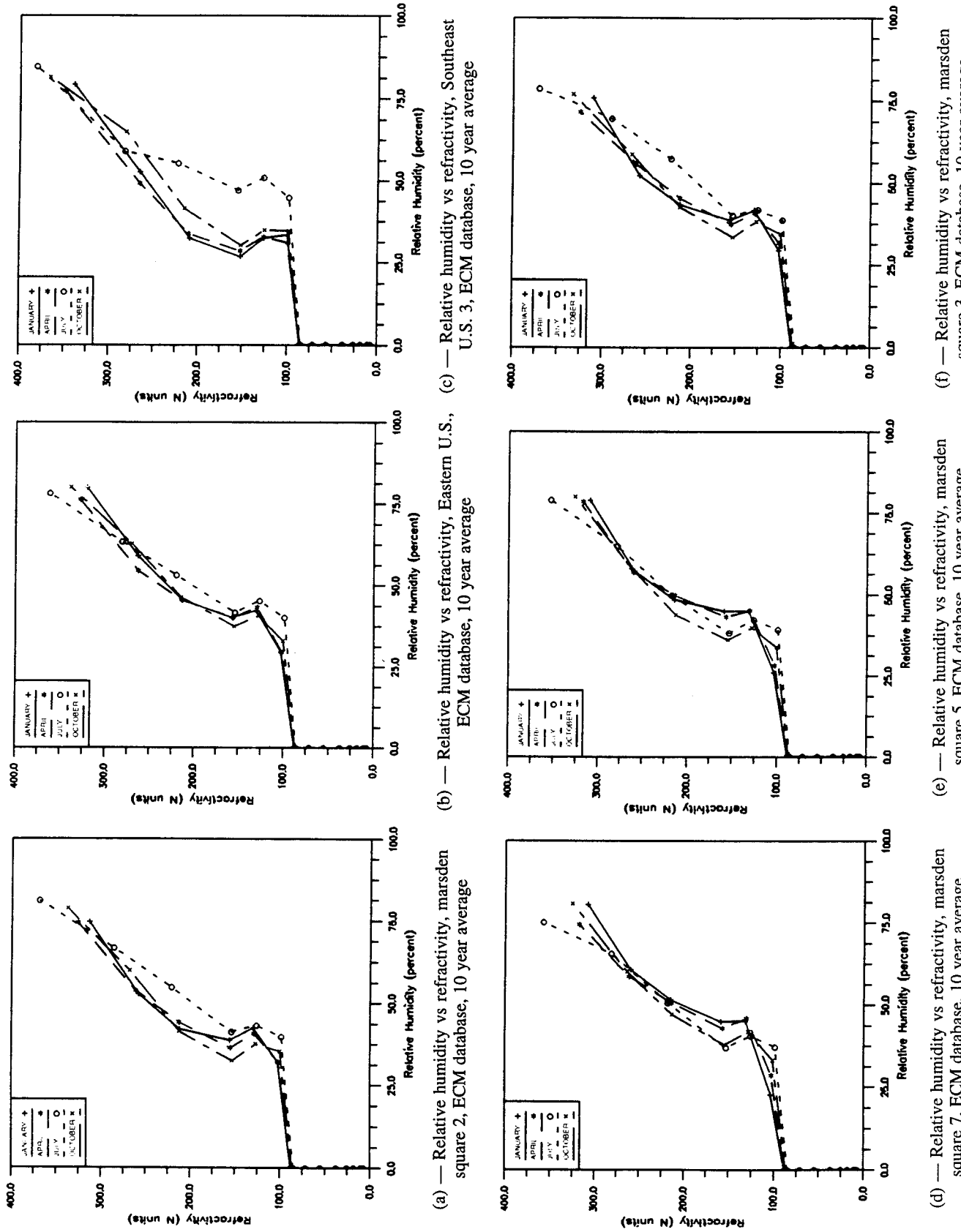

(a) — Relative humidity vs refractivity, marsden square 2, ECM database, 10 year average

(b) — Relative humidity vs refractivity, Eastern U.S., ECM database, 10 year average

(c) — Relative humidity vs refractivity, Southeast U.S. 3, ECM database, 10 year average

(d) — Relative humidity vs refractivity, marsden square 7, ECM database, 10 year average

(e) — Relative humidity vs refractivity, marsden square 5, ECM database, 10 year average

(f) — Relative humidity vs refractivity, marsden square 3, ECM database, 10 year average

Fig. 19 — Seasonal relative humidity vs refractivity over marsden squares 2, 3, 5, and 7, Southeast U.S., region 3, and Eastern U.S. region

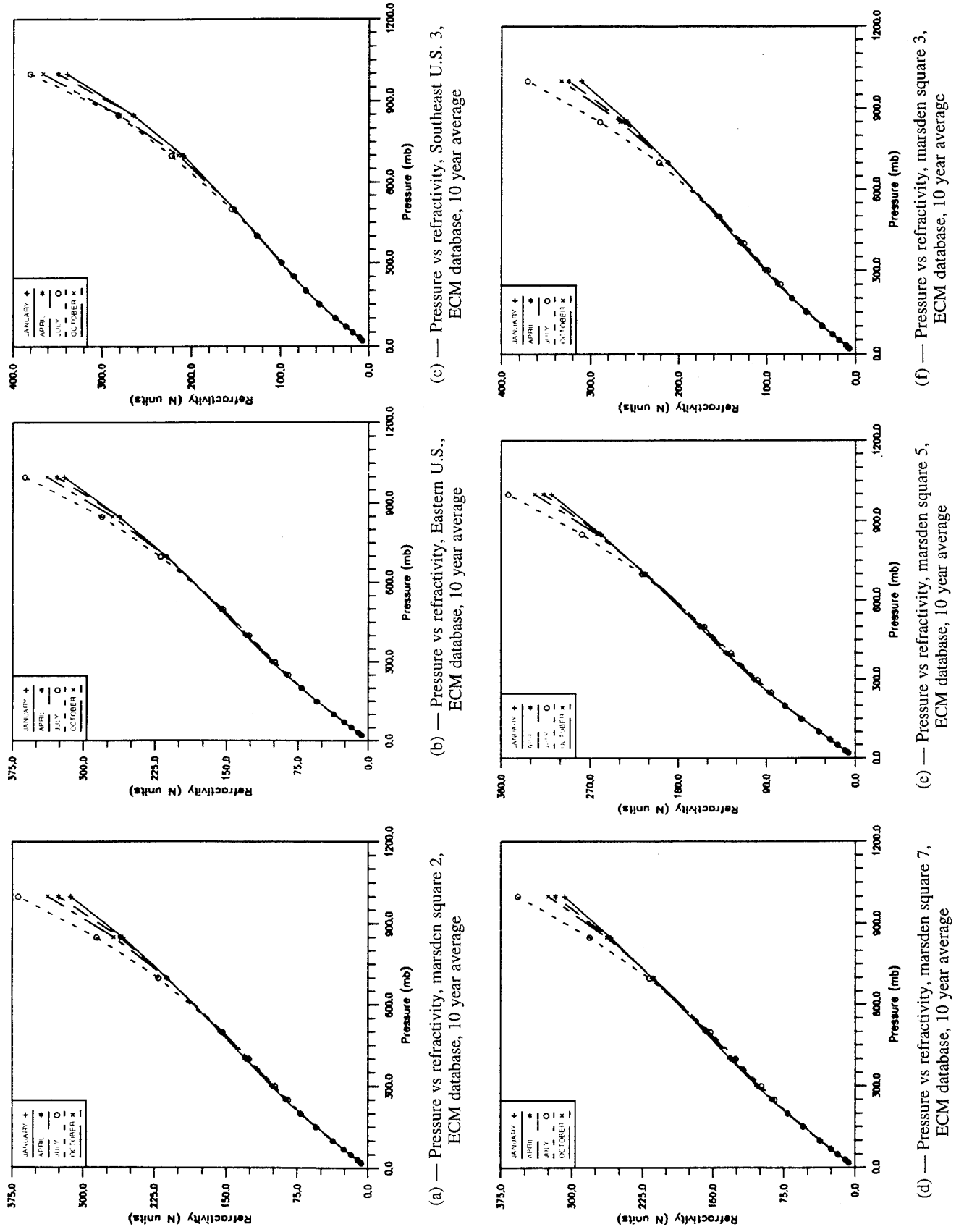

(a) — Pressure vs refractivity, marsden square 2, ECM database, 10 year average

(b) — Pressure vs refractivity, Eastern U.S., ECM database, 10 year average

(c) — Pressure vs refractivity, Southeast U.S. 3, ECM database, 10 year average

(d) — Pressure vs refractivity, marsden square 7, ECM database, 10 year average

(e) — Pressure vs refractivity, marsden square 5, ECM database, 10 year average

(f) — Pressure vs refractivity, marsden square 3, ECM database, 10 year average

Fig. 20 — Seasonal pressure vs refractivity over marsden squares 2, 3, 5, and 7, Southeast U.S., region 3, and Eastern U.S. region

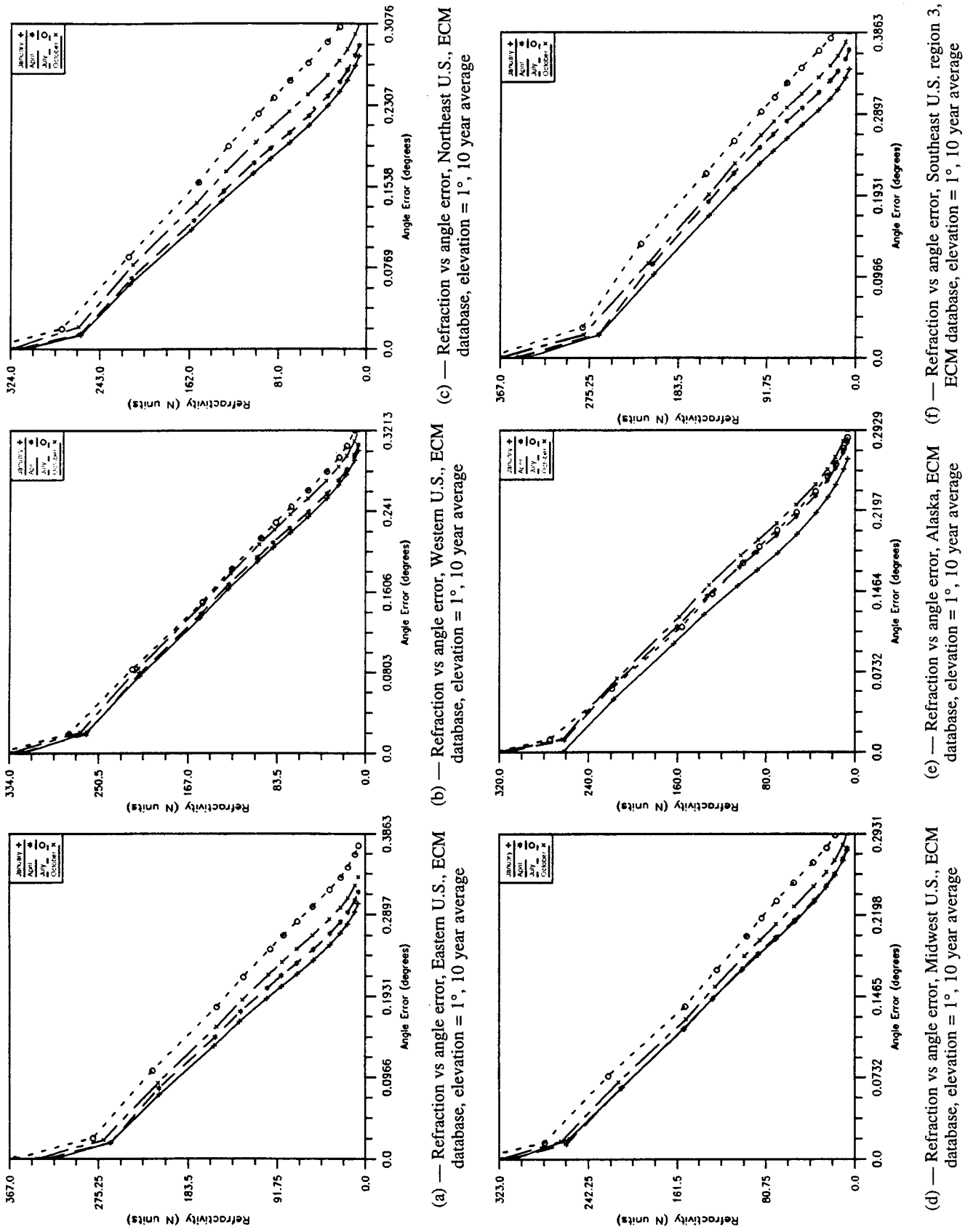

(a) — Refraction vs angle error, Eastern U.S., ECM database, elevation = 1°, 10 year average

(b) — Refraction vs angle error, Western U.S., ECM database, elevation = 1°, 10 year average

(c) — Refraction vs angle error, Northeast U.S., ECM database, elevation = 1°, 10 year average

(d) — Refraction vs angle error, Midwest U.S., ECM database, elevation = 1°, 10 year average

(e) — Refraction vs angle error, Alaska, ECM database, elevation = 1°, 10 year average

(f) — Refraction vs angle error, Southeast U.S. region 3, ECM database, elevation = 1°, 10 year average

Fig. 21 — Seasonal elevation angle errors vs refractivity for 1° apparent elevation angle over six U.S. regions including Alaska

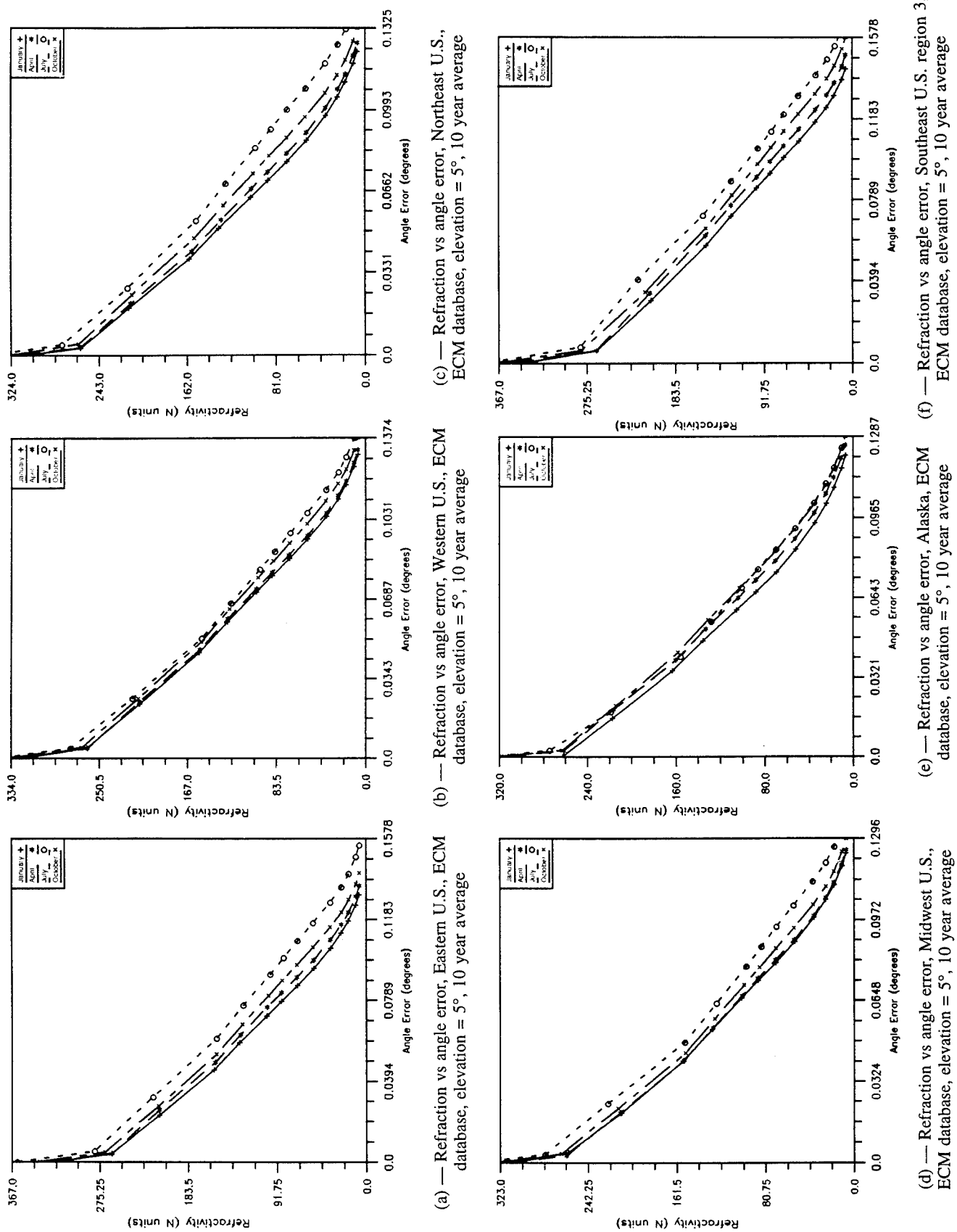

(a) — Refraction vs angle error, Eastern U.S., ECM database, elevation = 5°, 10 year average

(b) — Refraction vs angle error, Western U.S., ECM database, elevation = 5°, 10 year average

(c) — Refraction vs angle error, Northeast U.S., ECM database, elevation = 5°, 10 year average

(d) — Refraction vs angle error, Midwest U.S., ECM database, elevation = 5°, 10 year average

(e) — Refraction vs angle error, Alaska, ECM database, elevation = 5°, 10 year average

(f) — Refraction vs angle error, Southeast U.S. region 3, ECM database, elevation = 5°, 10 year average

Fig. 22 — Seasonal elevation angle errors vs refractivity for 5° apparent elevation angle over six U.S. regions including Alaska

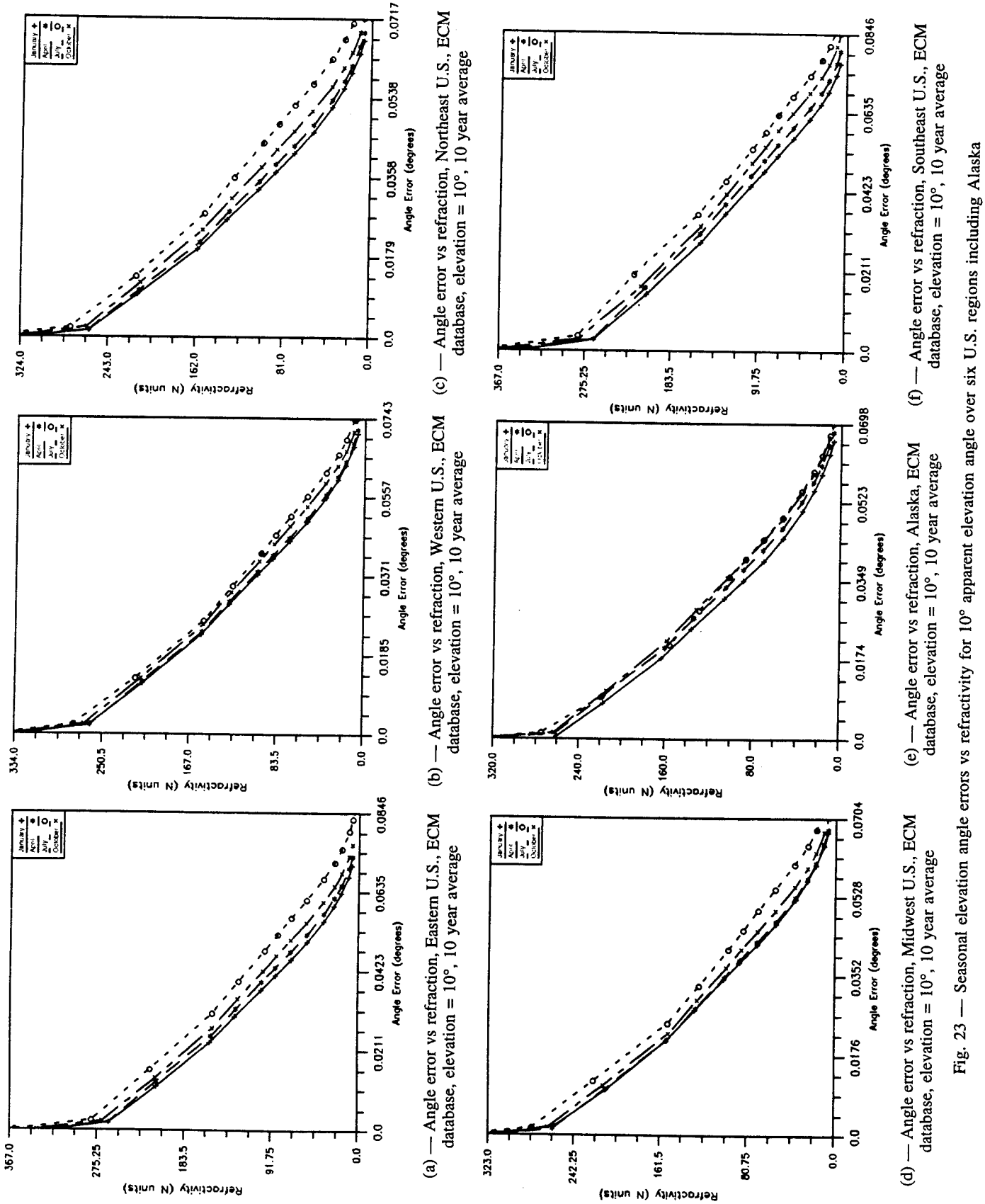

(a) — Angle error vs refraction, Eastern U.S., ECM database, elevation = 10°, 10 year average

(b) — Angle error vs refraction, Western U.S., ECM database, elevation = 10°, 10 year average

(c) — Angle error vs refraction, Northeast U.S., ECM database, elevation = 10°, 10 year average

(d) — Angle error vs refraction, Midwest U.S., ECM database, elevation = 10°, 10 year average

(e) — Angle error vs refraction, Alaska, ECM database, elevation = 10°, 10 year average

(f) — Angle error vs refraction, Southeast U.S., ECM database, elevation = 10°, 10 year average

Fig. 23 — Seasonal elevation angle errors vs refractivity for 10° apparent elevation angle over six U.S. regions including Alaska

Figures 24 through 26 show relational graphs between refractivity and range errors for 1°, 5°, and 10° apparent elevation angles over the six regional areas of the U.S. for four seasons as in the case of elevation angle errors. Range errors are about 72 to 82 m for 1° elevation angle over all six regions in the U.S. (Fig. 24), and these errors for 5° elevation angle are reduced to 28 and 30 m—40% of the lower errors for 1° elevation angle as shown in Fig. 25. Finally, range errors for 10° to 15 m—20% of the errors for the 1° elevation angle cases as in Fig. 26. This implies that range errors at 10° elevation angle are not reduced to single digit range errors over the entire U.S. regions for four seasons. In other words, apparent elevation angle should be higher than 10° in order to obtain a single digit range error i.e., few meters.

Finally, Fig. 27 shows a graph for the correlation between propagation time delay and the elevation angle over the entire U.S. region for the four seasons. For the given elevation angle, the propagation time delay varies over the regions and by season. As can be seen from Fig. 27, time delay in July is higher than those of any other month or season for all regions in the U.S. Minimum time delay at 5.5° is still higher than 84 ns, which is greater than acceptable limits in real environment applications. Figure 28 shows an extended graph of Fig. 27 from 6° to 15° elevation angle against the propagation time delay. As noted in Fig. 28, propagation time delay reaches 33 ns at 15° elevation angles. This implies that apparent elevation angle should be maintained above 15° to hold down the propagation time delay at the level of 30 ns or less.

CONCLUSIONS

Fundamentals of refractive index and lapse rate are introduced with interrelations of range and angle errors. Most of the approaches are here emphasized based on empirical data and ray-tracing algorithms. Temperature profiles show that local and seasonal or preferably diurnal data provide more accurate lapse rate information than global climatological data used. Refractivity variations described in this report show that refractivity variations are noticeably different along the latitude level at lower atmosphere than those on the upper atmosphere. Dynamic behavior of refractivity can be studied by investigating refractivity gradients of the first and second order with the histogram of Figs. 7 and 8. Several parametric analyses have been presented for range and elevation angle errors with respect to height, elevation angle, refractivity, local and regional bases. Range errors in the lower elevation angles (≤1°) are in the range of 80 m or above and at about 8 m for 15° elevation angles. Notice that range errors vary seasonally from a few meters to 10 m as well as monthly and locally. Elevation angle errors vary dynamically throughout the seasons and regional areas especially in the low elevation angles (≤6°). Additional results of correlations between refractivities and meteorological parameters have been presented to study direct effects of individual parameters against refractivity. It has been also noted that correlation between relative humidity and refractivity is more dynamic than that of pressure and temperature. Finally, results show that a minimum level of range error and elevation angle error can be obtained in the neighborhood of 12° to 15° of apparent elevation angles rather than 5° elevation angle, which most scientists have presented previously. Error analysis for diurnal and broader regional aspects will be investigated in the future with more relational functions in the sublow elevation angles (≤1°) and higher elevation angles (≥15°).

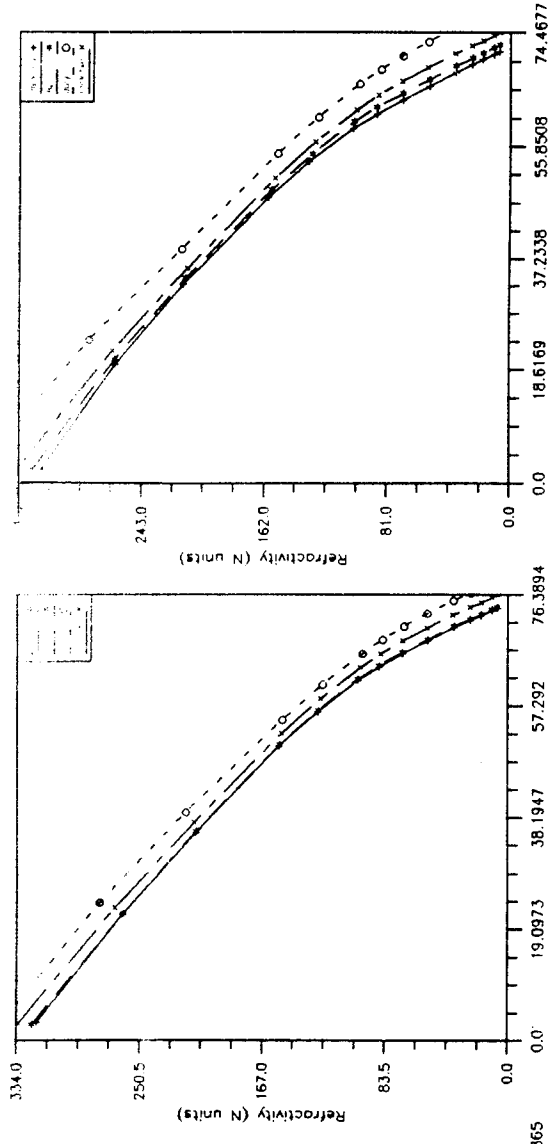

(a) — Refraction vs range error, Eastern U.S., ECM database, elevation = 1°, 10 year average

(b) — Refraction vs range error, Western U.S., ECM database, elevation = 1°, 10 year average

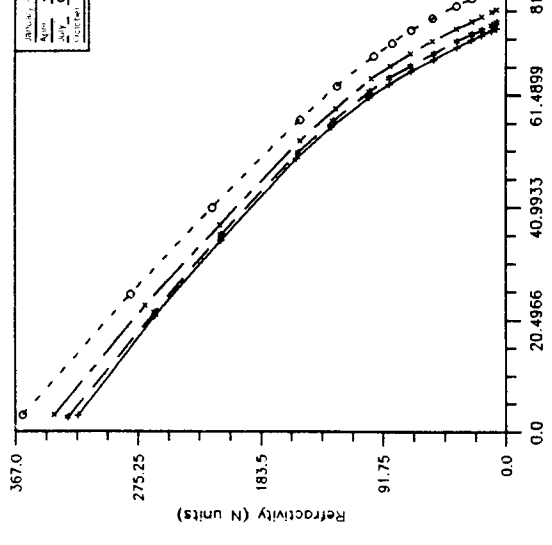

(d) — Refraction vs range error, Midwest U.S., ECM database, elevation = 1°, 10 year average

(c) — Refraction vs range error, Northeast U.S., ECM database, elevation = 1°, 10 year average

(e) — Refraction vs range error, Alaska, ECM database, elevation = 1°, 10 year average

(f) — Refraction vs range error, Southeast U.S. region 3, ECM database, elevation = 1°, 10 year average

Fig. 24— Seasonal range errors vs refractivity for 1° apparent elevation angle over six U.S. regions including Alaska

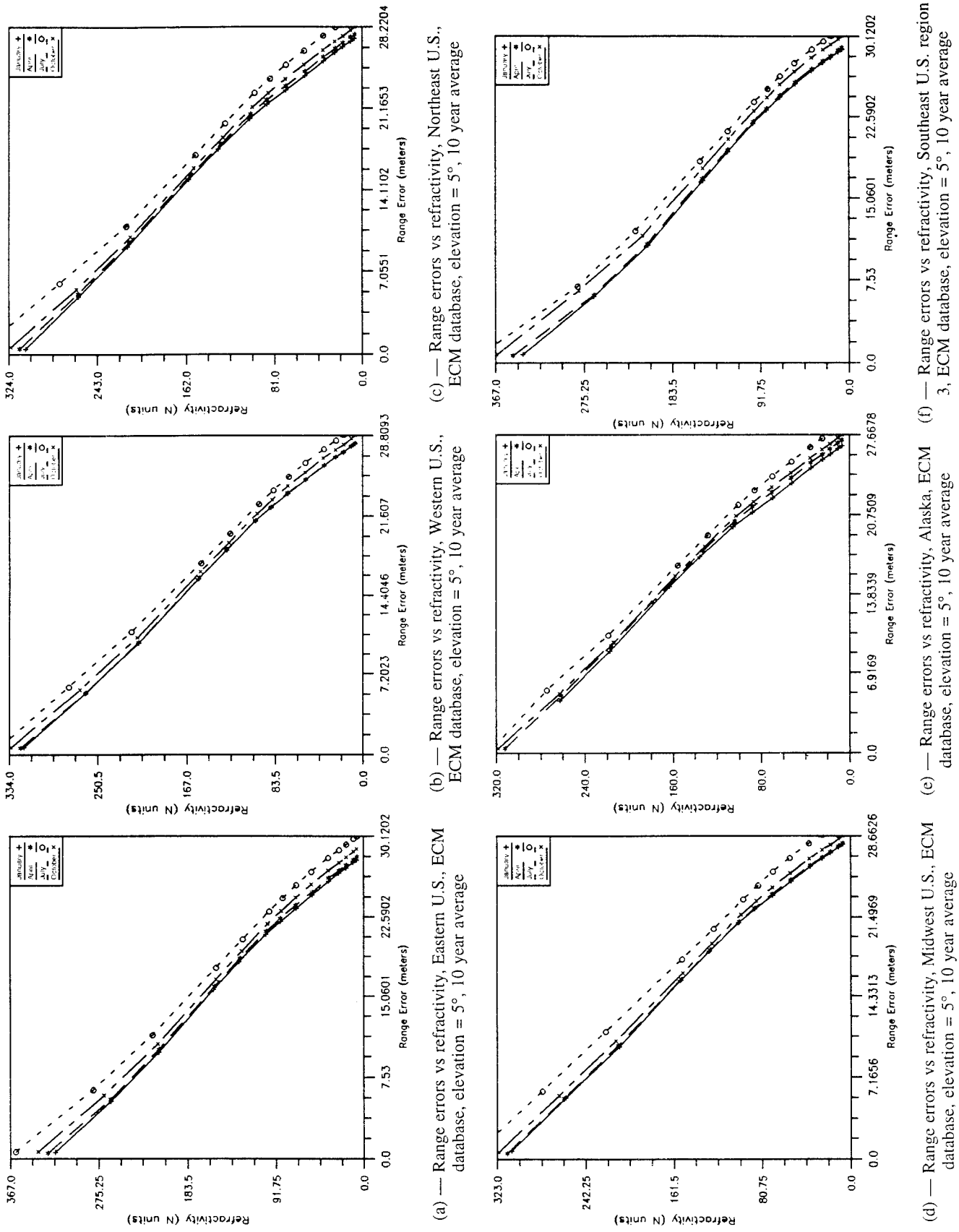

(a) — Range errors vs refractivity, Eastern U.S., ECM database, elevation = 5°, 10 year average

(b) — Range errors vs refractivity, Western U.S., ECM database, elevation = 5°, 10 year average

(c) — Range errors vs refractivity, Northeast U.S., ECM database, elevation = 5°, 10 year average

(d) — Range errors vs refractivity, Midwest U.S., ECM database, elevation = 5°, 10 year average

(e) — Range errors vs refractivity, Alaska, ECM database, elevation = 5°, 10 year average

(f) — Range errors vs refractivity, Southeast U.S. region 3, ECM database, elevation = 5°, 10 year average

Fig. 25 — Seasonal range errors vs refractivity for 5° apparent elevation angle over six U.S. regions including Alaska

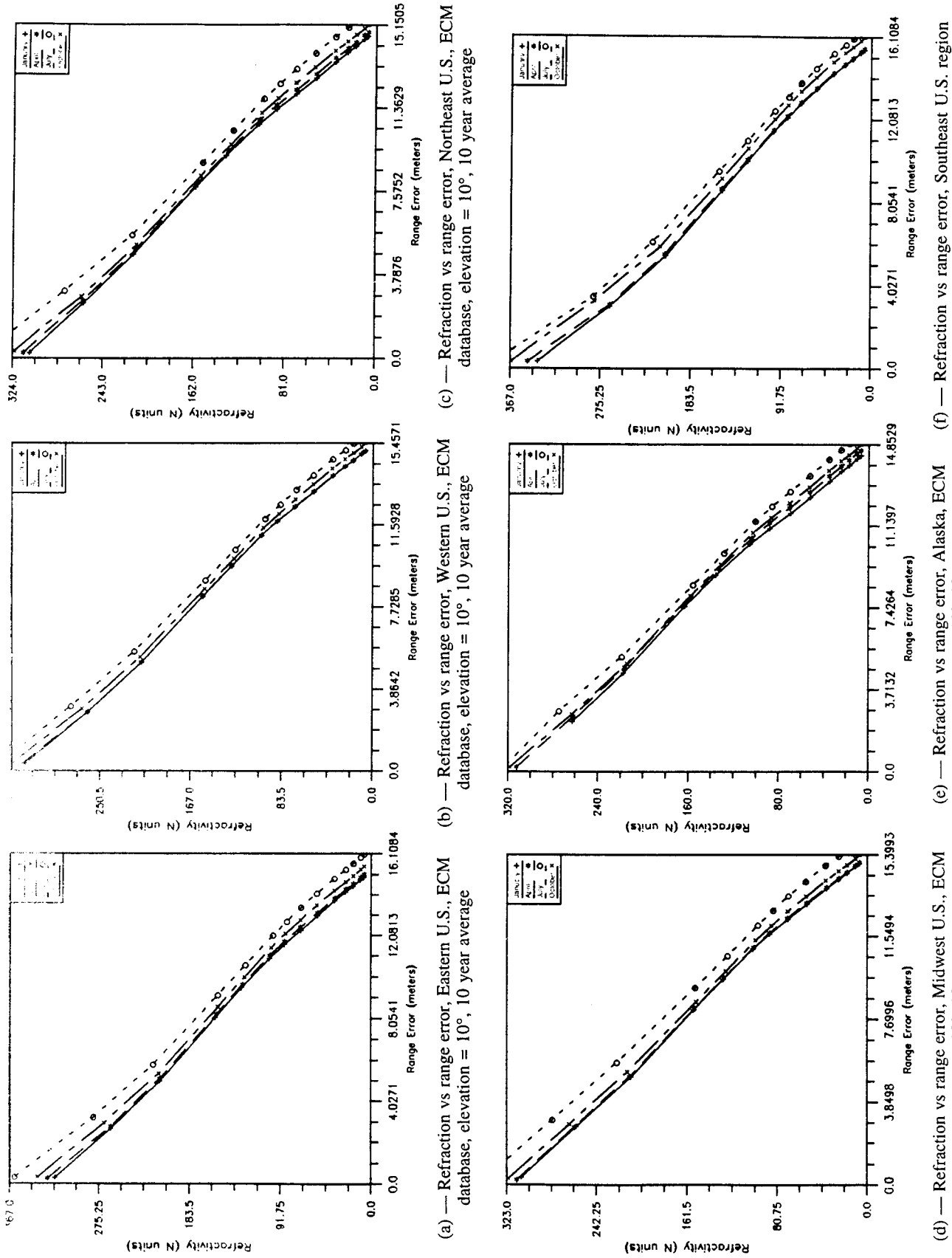

(a) — Refraction vs range error, Eastern U.S., ECM database, elevation = 10°, 10 year average

(b) — Refraction vs range error, Western U.S., ECM database, elevation = 10°, 10 year average

(c) — Refraction vs range error, Northeast U.S., ECM database, elevation = 10°, 10 year average

(d) — Refraction vs range error, Midwest U.S., ECM database, elevation = 10°, 10 year average

(e) — Refraction vs range error, Alaska, ECM database, elevation = 10°, 10 year average

(f) — Refraction vs range error, Southeast U.S. region 3, ECM database, elevation = 10°, 10 year average

Fig. 26 — Seasonal range errors vs refractivity for 10° apparent elevation angle over six U.S. regions including Alaska

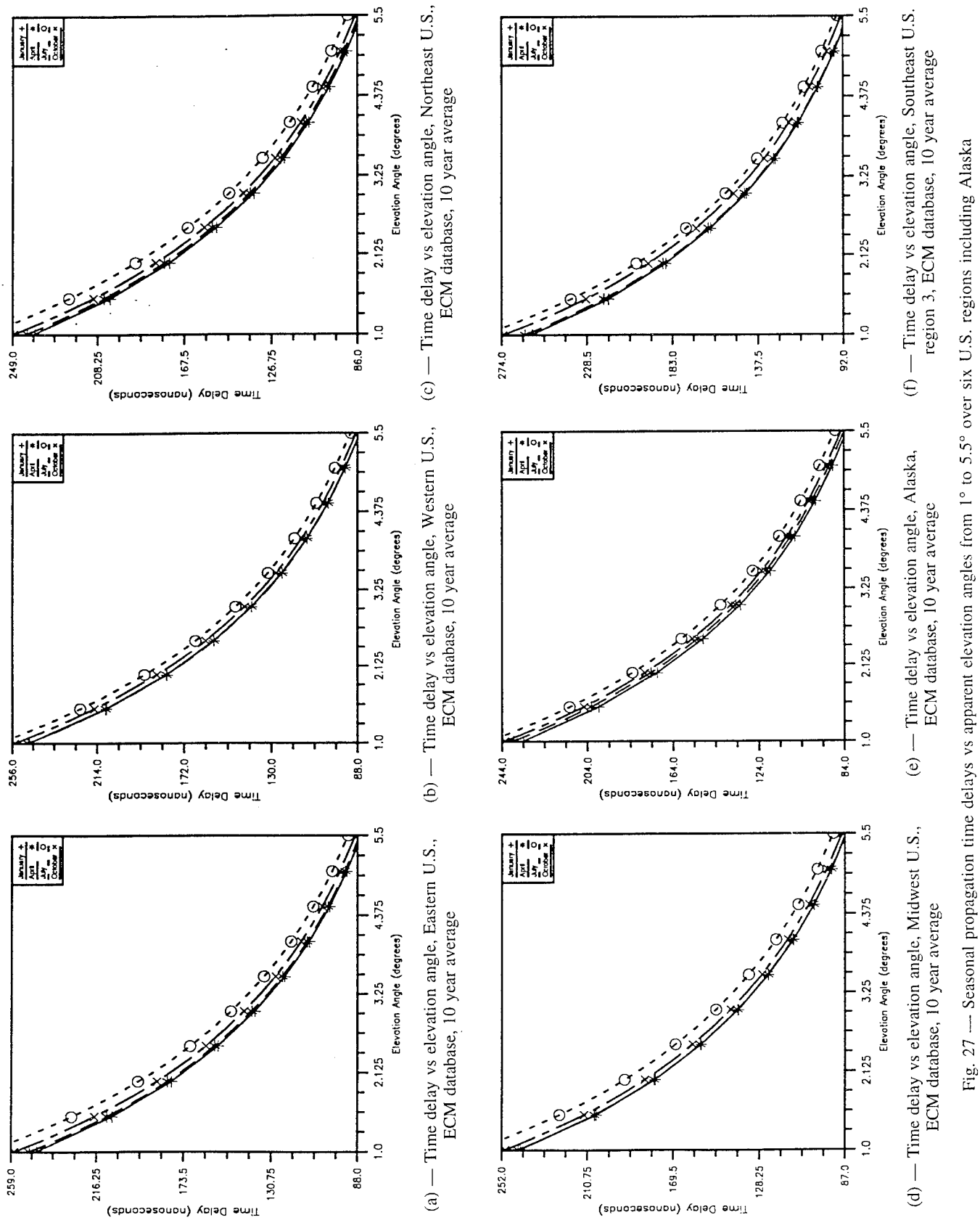

(a) — Time delay vs elevation angle, Eastern U.S., ECM database, 10 year average

(b) — Time delay vs elevation angle, Western U.S., ECM database, 10 year average

(c) — Time delay vs elevation angle, Northeast U.S., ECM database, 10 year average

(d) — Time delay vs elevation angle, Midwest U.S., ECM database, 10 year average

(e) — Time delay vs elevation angle, Alaska, ECM database, 10 year average

(f) — Time delay vs elevation angle, Southeast U.S. region 3, ECM database, 10 year average

Fig. 27 — Seasonal propagation time delays vs apparent elevation angles from 1° to 5.5° over six U.S. regions including Alaska

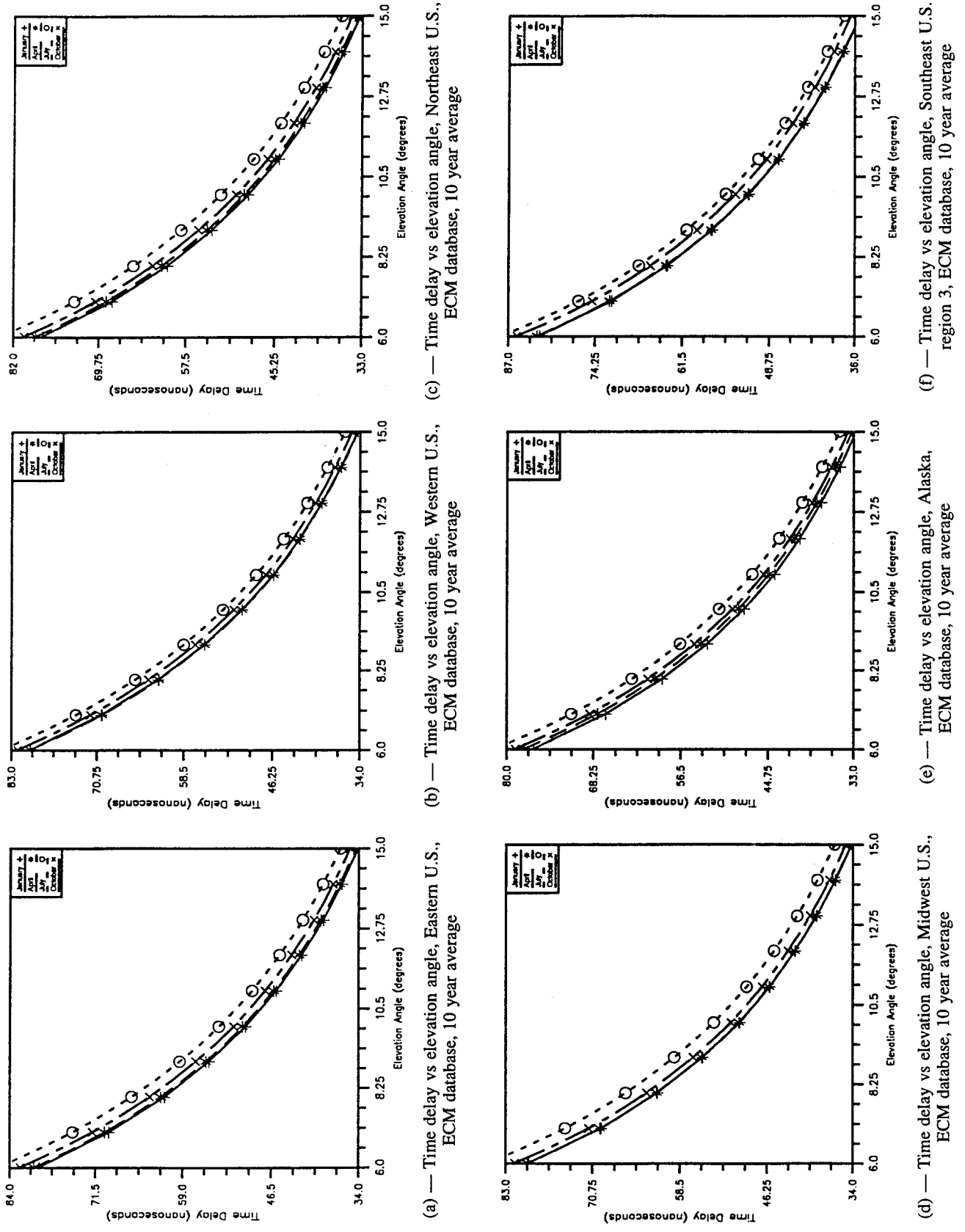

(a) — Time delay vs elevation angle, Eastern U.S., ECM database, 10 year average

(b) — Time delay vs elevation angle, Western U.S., ECM database, 10 year average

(c) — Time delay vs elevation angle, Northeast U.S., ECM database, 10 year average

(d) — Time delay vs elevation angle, Midwest U.S., ECM database, 10 year average

(e) — Time delay vs elevation angle, Alaska, ECM database, 10 year average

(f) — Time delay vs elevation angle, Southeast U.S. region 3, ECM database, 10 year average

Fig. 28 — Seasonal propagation time delays vs apparent elevation angles from 6° to 15° over six U.S. regions including Alaska

REFERENCES

1. Derr, V.E., "Remote Sensing of the Troposphere," Wave Propagation Laboratory, Boulder, CO, USA (U.S. GPO, Washington, DC), Aug. 1972.

2. Hopfield, H.S., "Two-Quartic Tropospheric Refractivity Profile for Correcting Satellite Data," *J. Geophy. Res.* **74**(18), 4487-4499 (1969).

3. Blake, L.V., "Ray Height Computation for a Continuous Nonlinear Atmospheric Refractive-Index Profile," *Radio Science* **3**(1) (1968).

4. Bean, B.R. and E.J. Dutton, "Radio Meteorology," National Bureau of Standards Monograph 92, March 1966, U.S. GPO, Washington, DC.

5. Campen, C.F. and A.E. Cole, "Tropospheric Variations of Refractive Index at Microwave Frequencies," Airforce Cambridge Research Center, Tech. Memo. #AFCRC TM-55-226, Oct. 1955.

6. Millman, G.H., "Atmospheric Effects on Radio Wave Propagation," in *Modern Radar: Analysis, Evaluation and Design*, R.S. Berkowitz, ed., (John Wiley & Sons, Inc., New York, 1965), Ch. 1, pp. 317-378.

7. Goad, C.C. and Lt. L. Goodman, "A Modified Hopfield Tropospheric Refraction Correction Model," Proc. of Amer. Geophy. Union, Fall Annual Meeting, San Francisco, CA, Dec. 1974.

8. Black, H.D., "An Easily Implemented Algorithm for the Tropospheric Range Correction," *J. of Geo. Res.* **83**(84), 1825-1828 ( ).

9. Yionoulis, S.M., "Algorithm to Compute Tropospheric Refraction Effects on Range Measurements," *J. of Geo. Res.* **75**(36), 7636-7637 (1970).

10. Webster, A.R., "Angles of Arrival and Delay Times on Terrestrial line of sight Microwave Links," IEEE Trans. on Antenna and Propagation **AP-31**(1), pp. 12-17 (Jan. 1993).

11. Choi, Junho, M. Melton, J. Donohue, and A. Frydland. "Analysis of Tropospheric Propagation Characteristics Based on Regional Meteorological Data," NRL Memo. Report, #NRL/MR/8140-95-7654, Feb. 1995.

12. Grossman, R.L.,"Atmospheric Environment," in *Remote Sensing of the Troposphere*, V.E. Derr, ed., NOAA, (U.S. GPO, Washington, DC, Aug. 1972), Ch. 1, pp. 1-1 - 1-27.

13. Bean, B.R. and J.D. Horn, "The Radio Refractive Index near the Ground,", *J. of Res.*, National Bureau of Standard **63D**(3) (Radio Propagation), 259-273 (Nov.-Dec. 1959).

14. Baird, R.C., "RF Measurements of the Speed of Light," Proc. IEEE **55**(6), June 1967, pp. 1032-1039.

15. Kerr, D.E., *Propagation of Short Radio Waves*, (McGraw-Hill, Inc., New York, 1951).

16. Bean, B.R. and G.D. Thayer, "Models of the Atmospheric Radio Refractive Index," Proc. IRE, **47**(5), 1959, pp. 740-755.

17. Smith, E.K. and S. Weintraub, "The Constants in the Equation for Atmospheric Refractive Index at Radio Frequencies," Proc. IRE, **41**(8), Aug. 1953, pp. 1035-1037.

18. "Meteorological Factors in Radiowave Propagation," Report of a Conference, 8 April 1946, Royal Institution, London, The Physical Society and The Royal Meteorological Society.

19. "Effects of Tropospheric Refraction on Radiowave Propagation," International Radio Consultative Committee (CCIR), **V**, Recommendation 453-2 (1970, 1986, 1990).

20. Patterson, W.L. et al., "Engineer's Refractive Effects Prediction System (EREPS) Revision 2.0," Naval Ocean Systems Center, Tech. Doc. #1342, Revision 2.0, Feb. 1990.

21. Thayer, G.D., "A Rapid and Accurate Ray Tracing Algorithm for a Horizontally Stratified Atmosphere," *Radio Science* , **1**(2), pp. 249 - 252 (Feb. 1967).

22. Weisbrod, S. and L.J. Anderson, "Simple Methods for Computing Tropospheric and Ionospheric Refractive Effects on Radio Waves," Proc. IRE, **47**(10), Oct. 1959, pp. 1770-1777.

23. Rowlandson, L G. and R.G. Moldt, "Derivation of Closed Functions to Compensate Range and Angle Errors in an Exponential Atmosphere," *Radio Science*, **4**(10), pp. 927-933 (Oct. 1969).

24. Crane, R.K., "Propagation Phenomena Affecting Satellite Communication Systems Operating in the Centimeter and Millimeter Wavelength Bands," Proc. IEEE, **59**(2), Feb. 1971, pp. 173-188.

25. Barton, D.K. and H.R. Ward, "Handbook of Radar Measurement," (Artech House, Boston, MA, 1969).

26. Allnut, J.E., "Satellite-to-Ground Radiowave Propagation: Theory, Practice and System Impact at Frequencies above 1 GHz," (Peter Peregrinus, Ltd., London, England, 1989).

27. Bean, B.R. and R.E. McGarvin, "A Review of Refraction Effects on the Apparent Angle of Arrival of Radio Signals," Propagation Factors in Space Communications, AGARD/NATO Avionics Panel, Ionospheric Research Committee, 10th Annual Symposium, Rome, Italy, A68-23069-07-07, Sept. 1965, pp. 529-546.

28. Bertram, S., "Compensating for Propagation Errors in Electromagnetic Measuring Systems," *IEEE Spectrum*, pp. 58-63, Mar. 1971.